

Modelling the European wind-blown dust emissions and their impact on PM concentrations

Marina Liaskoni¹, Peter Huszar¹, Lukáš Bartík¹, Alvaro Patricio Prieto Perez¹, Jan Karlický¹, and Ondřej Vlček²

¹Department of Atmospheric Physics, Faculty of Mathematics and Physics, Charles University, Prague, V Holešovičkách 2, 18000, Prague 8, Czech Republic

²Czech Hydrometeorological Institute, Na Šabatce 2050/17, 143 00 Prague 12, Czech Republic

Correspondence: Marina Liaskoni (marina-despoina.liaskoni@matfyz.cuni.cz)

Abstract. Wind-blown dust (WBD) emitted by the Earth's surface due to sandblasting can potentially have important effects on both climate and human health via interaction with solar and thermal radiation and reducing air-quality. Apart from the main dust "centers" around the world like deserts, dust can be emitted from partly vegetated middle and high latitude areas like Europe if certain conditions are suitable (strong winds, bare soil, reduced soil moisture, etc.). Using a ~~wind-blown~~ wind-blown 5 dust model (WBDUST) along with a chemical transport model (CAMx) coupled to a regional climate model (WRF), this study as one of the first ones provides a model based estimate of such emissions over Europe as well as the long-term impact of WBD emissions on the total PM concentrations for the 2007-2016 period.

We estimated WBD emissions to about 0.5 and 1.5 Mg yr⁻¹ km⁻² in fine and coarse mode in average. Maximum emissions occur over Germany where the average seasonal fine and coarse mode emission flux can reach ~~0.2 and~~ 0.5 and 1 g s⁻¹ km⁻², 10 respectively. Large variability is seen in the daily averaged emissions with values up to 2 g s⁻¹ km⁻² for the coarse mode aerosol on selected days.

The WBD emissions increased the modelled winter PM2.5 and PM10 concentrations by up to 10 and 20 µgm⁻³, respectively, especially over Germany, where the highest emissions occur. The impact on other seasons is lower. Much higher impacts are modelled however during selected days when occasionally the urban PM2.5 and PM10 concentrations are increased by more 15 than 50 and 100 µgm⁻³. The comparison with measurements revealed that if WBD is considered, the summer biases are reduced however the winter PM is even more overestimated (so the bias increased). We identified strong overestimation of the modelled wind-speed (the maximum daily wind is almost 2 times higher in WRF than the measured ones) suggesting that WBD emissions are also overestimated hence the enhanced winter PM biases.

Moreover, we investigated the secondary impacts of the crustal composition of fine WBD particles on secondary inorganic 20 aerosol (SIA): sulphates (PSO4), nitrates (PNO3) and ammonium (PNH4). Due to perturbing the water pH value and thus the uptake of their gaseous precursors as well as due to increased aerosol surface serving as oxidation site, we modelled increased seasonal PSO4 and PNO3 concentrations by up to 0.1 µgm⁻³ and decreases for PNH4 (by up to -0.05 µgm⁻³), especially during winter. As the average daily impact, these numbers can however reach much larger values up to 1-2 µgm⁻³ for sulphates and nitrates while the decrease of ammonium due to WBD can reach -1 µgm⁻³ on selected days. The sensitivity

25 test on the choice of the inorganic equilibrium model (ISORROPIA vs. EQSAM) showed that if EQSAM is used, the impact on SIA is slightly stronger (by a few 10%) due to larger number of cations considered for water pH in EQSAM.

Our results have to be considered as a first estimate of the long-term WBD emissions and the related effects on PM over Europe. Due to the strong positive wind bias and hence strong WBD emissions, we should consider these results as an upper bound. More sensitivity studies involving the impact of the driving meteorological fields, WBD model choice and the input data used to describe the land-surface need to be carried out in future to better constrain these emissions.
30

1 Introduction

Wind-blown dust (WBD) emitted by the Earth's surface can have a significant effect on both climate and human health by reducing air quality. It affects the climate directly and indirectly by scattering solar radiation, modifying the cloud properties and precipitation as it can also serve as cloud-condensation nuclei (Ryder et al., 2013; Song et al., 2022). Additionally, exposure 35 to high levels of dust particles can have severe effects on human health concerning the respiratory and the cardiac system (Giannadaki et al., 2014; Keet et al., 2018).

One of the major emitters of WBD of concern in Europe (but also globally) is the Sahara desert which contributes to 50% of dust emissions globally. Sahara dust is a major contributor to European atmospheric pollution as well, and its levels are critically high in southern Europe, while light dust episodes are often detected above Central and Western Europe (Wang et 40 al., 2020). Other natural sources can be wildfires, which due to intense turbulence can generate dust emissions (Wagner et al., 2018). WBD can be emitted also by non-vegetated areas containing fine and loose sediments when strong winds occur. Human activities contribute significantly in the increasing dust generation too. Destruction of soil crust and vegetation removal in semi-arid regions, changing cultivation patterns and new transport pathways are some of the most affecting anthropogenic activities (Birmili et al., 2008).

45 During climate change, dust emissions are anticipated to increase in the future (Zittis et al., 2022). Modified climate conditions (with the associated weather patterns) and changes in land use are the main affecting factors. If dry periods between the precipitation events get prolonged, then the soil of the surface is going to be prone to strong winds, ending up in an increase in dust emissions. Gudmundsson et al. (2016) assessed how the anthropogenic contribution to the emissions has affected the probability of droughts in Europe. Their results stress that the drought risk for southern Europe has already increased, although 50 the results for Central Europe are inconclusive. Stagge et al. (2017) used two precipitation indices and showed significant increases in drought likelihood for southern Europe, and decreases in the total area of the north, resulting in values that are dependent on the geographical domain, and can shift the spatially-averaged values for whole Europe. On the other hand, many studies have shown that fine particles can be transported over long distances through the atmosphere and elevate PM levels in different areas of the continent, far from the area of source (Ansmann et al., 2003; Francis et al., 2022; Zwaafink et al., 55 2022). Hence, mineral dust emissions must be examined in connection to both the main dust centres (like the Sahara) but also those emitted over non-arid areas like Europe where normally the temporal distribution of precipitation and denser vegetation

prevents the necessary soil drying for such emissions. Indeed, as said above, within a changing climate, such conditions can be more frequent.

Over Europe, very few studies accounted for the local (i.e. not that advected from other continents) dust emissions. Recently, Meinander et al. (2022) identified potential dust sources over Europe (among other areas). Korcz et al. (2008) gave a detailed model based estimate for the spatial and temporal variation of such emission using a mesoscale weather model (MM5) as the meteorological driver. They however did not compute their contribution to the total PM concentrations. Vautard et al. (2005) calculated the emission from natural erosion and re-suspension over Europe and found significant model (CHIMERE) improvement when these emissions are accounted for PM they however considered only two seasons in a selected year without giving account for long-term effects. Similarly, Bessagnet et al. (2008) considered a strong European dust event originating in Ukraine, but this cannot be considered representative for long-term. Recently, Kakavas and Pandis (2021) looked at urban dust over Europe and calculated its impact on PM levels. Moreover, they also accounted for the impact on the formation of secondary aerosols. They showed that the urban dust source can be significant and can potentially reduce model biases. However, they were not interested in other dust sources, e.g. those originating from soils from rural/natural areas and they looked only at one month not providing a long term estimate.

Motivated by this, here we present a novel study to quantify the long-term dust emissions for present-day conditions over central Europe using a regional climate model coupled with a chemical transport model along with a WBD model for dust fluxes. For the correct modelling of potential future evolution of WBD it is crucial to first evaluate the models ability to resolve their present-day magnitude and the associated impact on the total PM concentrations. Our study focuses on the long-term impact during a 10y period which allows us to obtain a representative pattern of the temporal and spatial distribution of the WBD emissions and their overall impact on PM levels. Moreover, this study will also look at the secondary impact of WBD particles on secondary aerosol components focusing on the inorganic aerosol. Indeed, there is an indication that the composition of dust particles can have an indirect impact on nitrates, sulphates and ammonia (Fairlie et al., 2010; Karydis et al., 2011; Wang et al., 2012; Malagutti et al., 2015; Kakavas and Pandis, 2021; Wang et al., 2022) either by acting as a surface for heterogeneous reactions (e.g. Fu et al. (2016); Wang et al. (2022)) or by their ion composition and modulating aqueous reactions that form nitrates and sulphates (Kakavas and Pandis, 2021) representing an indirect pathway of impacting the overall PM levels. In this study, the main interest will be the quantification of WBD contribution to urban PM levels as urban areas already experience adverse air-pollution episodes and it is of interest to calculate how natural emissions like WBD can potentially contribute to urban PM concentrations.

85 2 Methods and data

To achieve the goals of the study, we applied the chemical transport model CAMx driven offline by regional climate model WRF. The emissions of wind-blown dust were calculated by the WBDUST emissions model. All these models are described in detail below.

2.1 Dust model

90 The dust emission scheme WBDUST used here is based on [?Klingmüller et al. \(2018\)](#) study, who updated a new dust emission scheme based on Astitha et al. (2012)'s approach. This scheme combines meteorological parameters with descriptions of land cover type, clay fraction of the soil, the vegetation cover, the topography factor and the chemical composition. From the landcover data, "barren or sparsely vegetated" grid fractions are identified as land capable of dust emissions. The clay fraction is used to calculate the sandblasting efficiency which increases exponentially with a clay fraction up to 20%, beyond that it is
95 considered constant. Another important parameter influencing the dust emissions is the amount of vegetation. Quantitatively it is expressed as the total area of the leaves relative to the surface area called Leaf Area Index(LAI). In the WBDUST model, no emissions are considered for $LAI > 0.35$ while full emissions occur at zero LAI with linear dependence between. In the dust module, LAI is converted to the vegetation factor (fveg) defined as:

$$f_{veg} = 1 - \frac{\min(LAI, 0.35)}{0.35} \quad (1)$$

100 Consequently, the vegetation factor takes values between zero and one, where zero value corresponds to full emissions (no vegetation) and one means no emissions (i.e. full vegetation). To avoid the situation where the average LAI over a gridcell is higher than 0.35 leading to zero dust emissions, although the gridcell may contain fractions with lower LAI that would otherwise emit some dust, we first converted LAI data into fveg data retaining the same resolution. Only after this step we
105 redistributed it into the model gridcell. With this approach, we accounted for the dust emittable surface fractions with limited vegetation. The maps on Fig. 1 represent the WBDUST input data, namely the clay fraction and the LAI converted vegetation factor for January and July, taken from the middle of the decade of interest (year 2010).

The emission flux for dust in size mode "i" in WBDUST is calculated by the following equation:

$$j_{emis,i} = \frac{c\rho_{air}}{g} (u_* + u_{*t})^2 (u_* - u_{*t}) 10^{-4} \alpha f_{landcover} f_{veg} M_i N S_{topo}, \quad (2)$$

110 where c is an empirical constant (here = 1.5), u_* is the surface friction velocity, u_{*t} is the threshold surface friction velocity, $f_{landcover}$ is the barren land fraction, f_{veg} is the vegetation factor, α is the sandblasting efficiency, ρ_{air} is the air density, g is the gravitational acceleration, M_i is the mass fraction emitted into the mode "i", N is the normalization factor and finally, S_{topo} is the topography factor parameter, which enhances the representation of emissions which are generated in valleys and basins. The equation for the threshold surface friction velocity can be found analytically in [?Klingmüller et al. \(2018\)](#).

115 WBDUST is based on Fortran and is provided as a preprocessing tool along with the CAMx code (<https://www.camx.com/download/support-software/>, last visited 30 Nov 2022). It is driven by WRF meteorological data (see below) while the required parameters are described in Section 2.4.

2.2 Driving meteorological model

To drive the dust model with meteorological data as well as to drive the chemical transport model used, the WRF (Weather Research and Forecasting) model version 4 (Skamarock et al., 2019) was used. In WRF, the radiation processes are parameterized by RRTMG scheme (Iacono et al., 2008), microphysical processes and convection were treated by Purdue Lin scheme (Chen and Sun, 2002) and the Grell-3D scheme (Grell, 1993), respectively. The description of surface layer processes followed the Eta model (Janjic, 1994). The land surface exchange is parameterized by the Noah (Chen and Dudhia, 2001) and, finally, the boundary-layer is resolved by the BouLac planetary boundary layer scheme (Bougeault and Lacarrère, 1989). Static land-use data for WRF is derived from CORINE Land Cover data, version CLC 2012 (CORINE, 2012). For urban grid-boxes, the single-layer urban canopy model (SLUCM;(Kusaka et al., 2001)) is used with the same urban parameters as in Karlický et al. (2018). The choice of physical parameterizations is based on results from Karlický et al. (2020) who performed a series of sensitivity experiments to achieve the best possible model-observation agreement. To drive the regional climate in WRF, the ERA-interim reanalysis (Simmons et al., 2010) was used.

2.3 Chemical transport model

To account for the transport of the emitted dust and its interaction with the aerosol physical and chemical processes we used the chemical transport model CAMx version 7.10 (Comprehensive Air-quality model with Extensions; Ramboll et al. (2020)). CAMx is an Eulerian chemical transport model that simultaneously treats photochemistry and aerosol processes. As gas-phase chemistry and secondary aerosol formation are closely linked and, moreover, in our study we are interested in the impact of dust on secondary inorganic aerosol, we considered the “full” gas-phase chemistry in CAMx using the CB6r5 mechanism (Carbon Bond revision 6) described in Yarwood et al. (2010) and Emery et al. (2015).

For aerosol, a static two-mode (fine/coarse) approach called CF2E is adopted. Secondary inorganic aerosol is partitioned between gas and aerosol phases using either the ISORROPIA thermodynamic equilibrium model v1.7 (Nenes et al., 1998, 1999) or the EQSAM (EQilibrium Simplified Aerosol Model V4) model (Metzger et al., 2016). ISORROPIA considers sulphate (PSO_4), nitrate (PNO_3), chloride (NCL), ammonium (PNH_4), and sodium (NA), with an update for calcium nitrate on dust particles, which is important for our study. Aqueous nitrate and sulphate formation in cloud water is computed using the RADM-AQ aqueous chemistry algorithm (Chang et al., 1987) with updated sulphur dioxide (SO_2) oxidation reaction rates and metal-catalysed oxidation mechanism. A semi-volatile equilibrium scheme called SOAP (Strader et al., 1999) is used to form secondary organic aerosol from condensable vapours.

Apart from the secondary (in)organic aerosol, primary elemental (PEC) and organic carbon (POA), CAMx further considers general primary aerosol categories for fine crystal (dust; FCRS) and other fine primary aerosol (FPRM) and also for their coarse counterparts (CCRS and CPRM). The two mode CF2E approach optionally includes eight explicit fine-mode elemental species iron (Fe), manganese (Mn), calcium (Ca), Mg, K, aluminium (Al), silicon (Si) and titan (Ti) which can be either modelled or background values are used for chemical calculations. Calcium is an exception, which is scaled from FCRS and FPRM.

The species FPRM, FCRS, CPRM, CCRS including the 8 elements do not chemically decay. However, light scattering by them along with other PM components affecting photochemistry is considered. Furthermore, the fine-mode species concentrations influence PM and heterogeneous gas chemistry. In RADM-AQ, the oxidation of SO_2 to sulphate is catalytically enhanced by Fe and Mn while Mg, Ca and K affect cloud pH hence the solubility of SO_2 . Further Mg, Ca and K influence inorganic aerosol partitioning in EQSAM and Ca reacts with HNO_3 soil dust particles to form calcium nitrate (CaNO_3) in ISORROPIA. Fine aerosol species FPRM and FCRS along with the 8 elements represent surface area for heterogeneous reactions of SO_2 and N_2O_5 . Uptake of SO_2 and HNO_3 by dust particles is also considered using a humidity-dependent uptake coefficient (Zheng et al., 2015).

CAMx was driven using WRF output translated to CAMx meteorological inputs using the wrfcamx preprocessor that is supplied along with the CAMx code <http://www.camx.com/download/support-software.aspx> (last access: 25 Nov 2022). The coefficients of vertical eddy-diffusion (K_v) are diagnosed in wrfcamx based on the similarity method adopted from the CMAQ model (Byun and Ching, 1999). The choice of the method for the calculation of K_v is crucial as it greatly determines the species vertical transport, especially over urban environments (Huszar et al., 2020). They further showed that the CMAQ method represents a mid-range of the K_v intensities diagnosed from WRF output.

2.4 Experiments and data

A series of model simulations using CAMx coupled offline to WRF were carried out over a "larger" central European domain of size 189×165 (from France to Ukraine, northern Italy to Denmark) at $9 \text{ km} \times 9 \text{ km}$ horizontal resolution centered over Prague (Czechia) (50.075N , 14.44E , Lambert conic conformal projection). WRF has 40 layers in vertical reaching 50hPa with the lowermost layer about 30 m thick. CAMx uses 18 layers with the top one at about 10 km. As long term impact of WBD emissions is analysed here, we covered a 10yr simulation period from 2007/01/01 to 2016/12/31.

As already said, WRF was driven with the ERA-Interim reanalysis while for CAMx chemical initial and boundary conditions we choose the CAM-Chem global model data (Buchholz et al., 2019; Emmons et al., 2020).

As anthropogenic emissions, the TNO-MACC-III data (an update of the MACC-II version; Kuenen et al. (2014)) were used from 2011 for the whole period. This high resolution ($1/8^\circ$ longitude $1/16^\circ$ latitude, roughly $6 \text{ km} \times 6 \text{ km}$) European emission database provides annual emission estimates for NO_x , SO_2 , non-methane volatile organic compounds (NMVOC), methane (CH_4), ammonia (NH_3), carbon monoxide (CO) and PM10 and PM2.5 in 11 activity sectors. The annual emission totals were redistributed to model grid-cells using the FUME (Flexible Universal Processor for Modeling Emissions) emission model (Benešová et al. (2018), <http://fume-ep.org/>, last access: 1 September 2022). FUME also took care of chemical speciation and time disaggregation of input, sector based emissions while the speciation and time disaggregation factors are based on Passant (2002) and van der Gon et al. (2011). The output of the FUME is CAMx-ready hourly emission data for the speciated model species. Biogenic emissions for CAMx are calculated offline with the MEGANv2.1 (Model of Emissions of Gases and Aerosols from Nature) model (Guenther et al., 2012) based on WRF meteorology and vegetation characteristics following Sindelarova et al. (2014).

For the WBDUST module, the inputs were the following. The land cover was described using the high resolution (100 m) CORINE CLC 2012 land cover data (<https://land.copernicus.eu/pan-european/corine-land-cover>; CORINE (2012)) in combination with the United States Geological Survey (USGS) database for gridcells with no information from CORINE. This
185 landuse was used also for CAMx dry-deposition scheme. The clay fraction data comes from the Global Soil Dataset for use in Earth System Models (GSDE; Shangguan et al. (2014)). The GSDE provides the clay fraction of the topmost 4.5 cm soil layer, which is most relevant for the sandblasting efficiency. Leaf-area-index data are taken from MODIS post-processed data provided by Yuan et al. (2011) at 30" resolution (around 500 m over our domain) with 8 day update interval. Year 2010 LAI was used for the whole period. As topography information to calculate the topography factor, the Global Multi-resolution Terrain
190 Elevation Data 2010 (GMTED, 2010) is being used, with a spatial resolution of 0.1°.

One of the important goals of the study is to examine the potential impact of WBD elemental composition (Na+, K+, Fe+, Mn+, Ca++ and Mg++) onto the formation of secondary inorganic aerosol. Therefore, we must also consider the chemical soil composition of the emitted dust. We estimated it based on fractions that were calculated by Karydis et al. (2011).

195 The emissions of ~~wind-blow~~wind-blown dust (with the model described above) were calculated for fine and coarse crustal material based on WRF output meteorology: surface temperature~~+~~+ soil moisture, snow water equivalent, wind, temperature, pressure and geopotential height of the two lowermost levels. WBD emissions were calculated thus on an hourly basis (in accordance with output frequency). The calculation was done for six elements (Ca, Fe, Mg, Mn, K and Na) while the mass fraction of fine dust that does not belong to any of the listed elements is emitted as general fine crustal material (FCRS). Coarse crustal material is also emitted as one general species CCRS.

200 In order to account for the sensitivity on the method for gas partitioning into the aerosol phase as well as due to the fact, that the CAMx crustal elements interact with aerosol chemistry differently, we conducted CAMx experiments for both the ISORROPIA and EQSAM equilibrium models. With each of these, a pair of experiments was conducted: i) one without considering WBD (~~only anthropogenic aerosol source and anthropogenic- and MEGAN-based including anthropogenic aerosol emissions as well as anthropogenic and biogenic~~ gas-phase emissions) and one ii) with WBD considered. The experiments are
205 named accordingly ISORROPIA_noWBD, ISORROPIA_WBD, EQSAM_noWBD and EQSAM_WBD.

210 In our analysis, we will examine the impact of WBD on PM2.5 and PM10 concentrations evaluated based on the ISORROPIA experiment pair. The EQSAM pair of simulations will be used to analyse the sensitivity of the impact secondary aerosol chemistry. It is clear that if dust particles influence the heterogeneous aerosol chemistry, the total contribution of WBD will be not simply the sum of concentrations of FCRS and the listed elements, but instead, we have to account for the effect dust has on secondary aerosol. Therefore the impact will be calculated as follows:

$$\Delta PM2.5 = PM2.5_{WBD} - PM2.5_{noWBD}, \quad (3)$$

while $PM2.5_{WBD}$ is calculated as

$$PM2.5_{WBD} = PEC + POA + FPRM + PSO4 + PN03 + PNH4 + SOA + FCRS + Ca + Fe + Mg + Mn + K + Na \quad (4)$$

$PM2.5_{noWBD}$ is calculated as

215 $PM2.5_{noWBD} = PEC + POA + FPRM + PSO4 + PNO3 + PNH4 + SOA + FCRS,$ (5)

while FCRS here stands for fine crustal material entering the domain through boundaries (it is not directly emitted within anthropogenic sources). For the impact on PM10, we added CPRM and CCRS to these sums to account for the anthropogenic and dust coarse mode aerosol, i.e.:

$$\Delta PM10 = (CCRS_{WBD} + PM2.5_{WBD}) - (CCRS_{noWBD} + PM2.5_{noWBD}). \quad (6)$$

220 Regarding $CCRS_{noWBD}$, as CCRS is not emitted in the noWBD simulations, this accounts for the crustal material entering the domain via the boundaries similar to FCRS above.

3 Results

3.1 Modelled WBD emissions

In this section, the dust emission fluxes calculated using the WBDUST emission module are analysed. The validation of the 225 underlying meteorological conditions driving the emission model as well as the resulting PM concentrations are validated in the next section.

In Fig. 2, the two maps represent the seasonal average emissions for winter, the season with highest emissions calculated. Winter averaged FCRS dust emissions have values that can reach up to ~~25-0.5~~ $gs^{-1}km^{-2}$ (grams per second per square km) while CCRS dust emissions can reach values that exceed ~~40-1~~ $gs^{-1}km^{-2}$. Increased emissions are noticed above western 230 Germany where many farmlands and agricultural areas are located. High emissions are also often concentrated around urban areas. Although the urban land-use category is not considered as bare soil, at the used resolution, many of the urban grid boxes are only partly covered by urban land cover (only a very few grid cells are covered by urban land cover by more than 50%) and the rest is usually a crop land which is potentially capable of dust emissions. As in the used LAI input (MODIS), it is often the cities, which have the sufficiently low LAI values (less than 0.35), it is there and over surrounding areas, where the conditions 235 for WBDUST emissions are met (low LAI and bare soil).

The seasonal variability was also assessed by calculating the average annual cycle of the monthly mean domain averaged emissions. Fig. 3 confirms that higher emissions occur in winter season for both FCRS and CCRS, while the main emitting period begins in October and ends in April, proving that the presence of winds along with low LAI are the governing factors for dust emissions.

240 The temporal variability of these emissions on a daily and hourly basis is shown in terms of the daily average values and the average diurnal cycle, respectively. Fig. 4 represents the time-series of the domain averaged daily averages. A high variability of daily emissions is seen and FCRS emissions can exceed ~~25-0.5~~ $gs^{-1}km^{-2}$ while CCRS emissions can reach values higher than ~~100-1~~ $gs^{-1}km^{-2}$ on specific days.

Fig. 5 shows the average diurnal cycle of the average hourly emission fluxes for different seasons. Emissions peak during
245 mid-day which is associated with stronger winds and usually lower stability enabling to lift the sandblasted soil to produce emissions. The daily amplitudes are about 0.5-1 ~~and 1-2~~ $\times 10^{-2} \text{ gs}^{-1} \text{ km}^{-2}$ ~~and 2-4~~ $\times 10^{-2} \text{ gs}^{-1} \text{ km}^{-2}$ for FCRS and CCRS, respectively.

3.1.1 Sensitivity to wind-speeds and LAI

Knowing the strong dependence of WBD emission fluxes to wind-speed values, we conducted two additional calculations. We
250 reduced wind-speeds entering the WBDUST model by a factor of 0.75 and 0.5 (motivated by the observed positive wind bias, see further).

We further also tested the sensitivity to LAI (via the derived vegetation factor, see Sec. 2.1) averaging from MODIS over
gridcells with urban land-cover fraction which, as already mentioned above, causes some locally increased WBD emissions
255 near urban areas. In our setup, about 400 MODIS LAI data points fall into one CAMx gridcell and we averaged LAI data only
for the non-urban fraction of a gridcell by excluding the fraction of lowest MODIS LAI values (usually zero) from averaging
that correspond to the urban fraction. In other words, we assumed that the higher LAI values within these 400 points are
associated with the non-urban gridcell fraction.

Results of these sensitivity tests are presented in Fig. 6 were the spatial distribution of winter WBD emissions are presented
for the default case as well as for the 0.75 and 0.5 reduction of wind-speeds and finally for the modified LAI averaging. For the
260 0.75 reduction, emissions are reduced and reach up to $10-15 \times 10^{-2} \text{ g s}^{-1} \text{ km}^{-2}$ with peaks up to $20 \times 10^{-2} \text{ g s}^{-1} \text{ km}^{-2}$. This
means that by 25% reduction of wind-speeds, emissions are reduced by a factor of 2 to 3. Going into a much stronger reduction
of 50% of the original wind-speeds, the resulting WBD emissions are reduced much more strikingly, i.e. by two orders of
magnitude and reach $30-50 \times 10^{-4} \text{ g s}^{-1} \text{ km}^{-2}$. This means that probably during many of the modelled days, the wind speed
values fell below the threshold friction velocity (u_*) resulting in zero emissions implying very low DJF average emissions.
265 Finally, for the modified LAI averaging we see that emission indeed decrease near cities (by about 50%) partly removing the
artificial emission peaks.

3.2 Validation

3.2.1 Meteorological fields

As the modelled wbdust emissions depend on meteorological conditions and the state of the soil, it is important to evaluate how
270 well the driving model (WRF) represents the meteorological conditions that affect emissions fluxes the most. In this section
we compare the modelled temperature and wind speed with available measurements from the area of Czech republic, while
the soil moisture will be compared with satellite data. Although it represents a small fraction of the entire domain, we expect
that the model biases are representative for larger areas. Measured temperature and wind data are from 10 Automated Immission
Monitoring (AIM; www.chmi.cz, last visited 30 NOV 2022) network air-quality monitoring stations that, besides air quality
275 data, provide also the basic meteorological variables.

Starting with the temperature, Fig. 7 represents the seasonal 2007-2016 averaged diurnal cycles. It is clear that the daily maximum temperatures are underestimated by the model during summer (JJA) while better match is achieved in other seasons. The autumn (SON) data show some positive model bias too. Regarding daily minima, the model tends to overestimate it for summer and autumn while a clear underestimate occurs in winter (DJF). The above mentioned biases are always less than 2°C
280 and usually less than 1°C.

As from dust emission perspective, the maximum wind speeds are more relevant than the average ones, we also compared the modelled monthly mean of the maximum daily wind speeds averaged over 2007-2016. Results are depicted in Fig. 8. It is clear that the model reasonably captures the annual cycle of wind with minima during late summer early autumn and maximum wind speeds during winter. However, a strong positive model bias is evident reaching 2-4 ms^{-1} , except the Praha-Ruzyně station and
285 Brno-Turany during summer.

Finally, the state of the soil in terms of moisture content is another key driver of emissions with low soil moisture promoting sand blasting and thus dust emissions. For this quantity, we used the ESA CCI SM v07.1 satellite based dataset (Dorigo et al., 2017; Gruber et al., 2019) and plotted the spatial distribution (for the area of Czechia) of the 2007-2016 seasonal means volumetric soil moisture, in Fig. 9. The satellite data shows a strong annual variation with minimum values during summer
290 (0-0.2 m^3m^{-3}) while much higher values during summer (0.4-0.6 m^3m^{-3}). This annual cycle is seen also in the modelled data but is much weaker with summer soil moisture data slightly lower than the winter ones. It is also clear that the model overestimates the observed data, especially during summer while the winter overestimation is small (with model values around 0.4-0.5 m^3m^{-3}) with even some underestimation limited to small regions.

3.2.2 PM concentrations

295 In this section, our results will be validated by comparing the modelled PM2.5 and PM10 concentrations calculated by CAMx (by the ISORROPIA experiment pair) with observations. The observations were retrieved from the European air quality database - Airbase (<https://discomap.eea.europa.eu/map/fme/AirQualityExport.htm>, last visited 30 NOV 2022; EEA, 2021) available "(sub)urban-background" stations from selected European cities (i.e. Vienna, Prague, Berlin, Munich, Budapest and Warsaw). These observations were plotted along with WBD and noWBD CAMx concentrations daily averaged for the 6 European cities for 2007-2016.
300

Fig. 10 and 11 depict daily time series for modelled and measured PM2.5 concentrations for selected European cities. In general, the time evolution of observed values is well captured by the model simulations. It is also seen that during summer months, concentrations are usually underestimated. For winter, when the highest measured peaks occur (often exceeding 100 μgm^{-3}), the model often fails to correctly capture the strength of the peak or its timing. It is also clear (and expected) that the
305 WBD simulation generates highest peaks which are closer to the observed peaks, or even exceeds those suggesting a positive model bias during winter. For PM10 (Fig. 12 and 13) the situation is similar in underestimating summer values while those for winter also often overestimated in the WBD simulation when very strong peaks occur (up to several 100 μgm^{-3} , e.g. for Prague, Munich or Warsaw reaching almost 500 μgm^{-3}) which are not seen in the noWBD simulation. This suggests probably a strong overestimation of the wind-blown dust emissions generating these peaks.

310 In Figures 14 and 15 the annual cycle of monthly mean concentrations for PM2.5 and PM10 are shown. All PM2.5 concentrations fluctuate with the same trend, having their highest values during winter and autumn seasons. The magnitude of the difference between the modelled data WBD and noWBD and the observations is around $5-10 \mu\text{gm}^{-3}$. Summer months are underestimated while the inclusion of ~~wind-blow~~ wind-blown dust reduces this negative bias. In winter the modelled values are overestimated in Munich and Prague while underestimated in Berlin, Budapest and Warsaw. Depending on this, the inclusion 315 of dust emissions increases (e.g. Prague, Munich) or decreases (Vienna, Warsaw, Budapest) the model bias. In case of PM10, summer values are underestimated in noWBD simulation by about $10-20 \mu\text{gm}^{-3}$, while this underestimation is clearly reduced for the WBD simulations to $0-10 \mu\text{gm}^{-3}$. A different situation occurs in winter, when the noWBD model values underestimate the measured data (by a similar magnitude as in summer), however, the inclusion of dust emissions increases model values such that a positive model bias is generated. This is in line with the daily time-series seen above when strong peaks occur in 320 the WBD simulation being probably the main cause of these seasonal biases.

To gain more quantitative information on whether the inclusion of ~~wbdust~~ WBD emissions reduced/enhanced the model biases, we calculated several statistical measures presented below.

In the Tab. 1 and 2, the Pearson correlation coefficient, the Root Mean Squared Error (RMSE) and the Normalized Mean Bias (NMB) were calculated for the daily mean concentrations of PM2.5 and PM10 in each city based on all values and on 325 seasonal selection. We calculated the statistics separately for WBD and noWBD ISORROPIA simulations.

The Pearson correlation measures the strength of the linear relationship between the modelled data and the observed one. RMSE is the standard deviation of the residuals (prediction errors). It tells how concentrated the data is around the line of best fit and lastly, finally, the Normalised Mean Bias (NMB) indicates the average deviation of the modelled values from the observed ones. These statistics are generated from all model-observation pairs from each station in a particular city.

330 The annual correlations of daily PM2.5 and PM10 with measurements are around 0.5-0.7 depending on the city, while the seasonal values are smallest for JJA around 0.2-0.4 and highest in DJF and MAM. An important result is that the correlations are much smaller for the WBD simulations, which indicates that the wind-blown dust emissions are poorly correlated with the real dust emissions that occurred. This is seen also for the RMSE, which has values between 5 and $20 \mu\text{gm}^{-3}$ for PM2.5 and between $10-40 \mu\text{gm}^{-3}$ for PM10 and evidently, the WBD values are higher. On a seasonal level, the lowest RMSE are 335 encountered for JJA. In case of mean bias, annual values for PM2.5 are up to -0.2 for the noWBD simulations. In this case, the WBD brought improvement for some cities resulting in lower absolute NMB. This is especially due to JJA values where NMB improved for all cities. For PM10, annual NMB are also negative and reach -0.37. The WBD annual NMBs are in this case also lower for almost each city compared to the noWBD values. On seasonal levels, the improvement, i.e. lower mean biases are also evident.

340 The result rise the question whether strong winds in WRF are responsible to overestimated WBD emissions and consequently PM concentration. To test this hypothesis, we chosen Prague and selected those days when the model bias is positive and larger than $50 \mu\text{gm}^{-3}$ (see Fig. 12). Then we used this mask and repeated the wind-comparison from Section 3.2.1 but selecting only the stations in and around Prague and averaging only over such days. The results are depicted in Fig. 16 for four stations. From the figure, it is clear that wind-speeds for such days are larger than the average for all days and reach values about 10-12

345 m.s⁻¹, which are about 50% higher than the averages for all days seen in Fig. 8. The bias however remained similar, i.e. the modelled wind-speeds are higher than the observed ones by 50-100%. This means that the relative bias of model winds retained its magnitude throughout all days in the examined period. However, in Fig. 6 we showed a very strong sensitivity of WBD emissions on wind-speed and a 50% change can significantly change the emission magnitude and thus concentrations of PM.

350 In summary, by including wind-blown dust emissions, the correlation of the daily PM2.5/10 values decreased strongly, and the RMSE increased. ~~However, the NMB improved~~ This can be explained by the many outliers in the modelled PM data. Both the correlation and the RMSE is very sensitive to such values. For NMB, improvement was achieved for PM10 for almost all seasons and cities, while for PM2.5, the improvement occurred only for summer months. ~~In overall it seems that model skill is deteriorated when WBD emissions suddenly increase due to strongly overestimated winds.~~

3.3 Impact of WBD emissions on PM

355 In this section, the spatial distribution and the temporal evolution of the impact of dust emissions on PM2.5 and PM10 concentrations is presented (i.e. the $\Delta PM2.5$ and $\Delta PM10$ from Eq. 3 and 6). Starting with the temporal evolution, Fig. 17 and 18 represent the WBD impact to PM2.5 and PM10 concentrations for selected cities in central Europe.

360 The WBD impact to PM2.5 daily urban concentrations can reach values up to 30 μgm^{-3} , where the highest values are noticed in Berlin contributing up to 60 μgm^{-3} to the total PM2.5 concentrations. The corresponding WBD impact to the PM10 concentrations are higher as expected and can reach values more than 80 μgm^{-3} , with Berlin representing again the highest extremes with values up to 200 μgm^{-3} . It is also clear that the highest impacts on PM are modelled during winter time in accordance with the annual cycle of emissions seen earlier.

365 To obtain spatial information on the WBD impact on PM, Fig. 19 depicts the seasonal averaged (2007-2016) dust impact on PM2.5 (left; $\Delta PM2.5$) and PM10 (right; $\Delta PM10$) concentrations above central Europe. The dust contribution to PM2.5 concentrations can reach values up to 12 μgm^{-3} in DJF and about 8 μgm^{-3} in other seasons while the highest impacts are modelled over Germany and over central Europe near large urban areas. In winter, a large part of the domain exhibits impact above 1 μgm^{-3} . The impact on PM10 is characterised with higher values up to 20 μgm^{-3} , mainly during DJF, while the spatial distribution is very similar to the PM2.5 impact being highest above western Europe (mainly Germany) with values above 2 μgm^{-3} over other areas. The impacts seen are in line with the highest emissions calculated in Fig. 2.

370 To further support the hypothesis, that the peak values in the daily concentrations seen in PM10 (Fig. 13 and 12) as well as in the impact figures (Fig. 18), we present the scatter plot of the daily mean concentrations of PM10 values above Prague vs. the WBD emissions from around this city (average of 10 x 10 gridcells) in Fig. 20. The two color distinguish concentration values below and above the 100 μgm^{-3} threshold. The figure shows that for values below this threshold, high concentrations are obtained even for very low WBD emissions which is probably a result of anthropogenic emissions. However, for high concentrations (blue color), it is clear that they correlate with the emissions of wind-blown dust.

3.3.1 Impact on PM components

As mentioned above, PM2.5 concentrations contain secondary constituents and in this section, we investigate how the presence of ~~wind-blow~~wind-blown dust (FCRS and elements Ca, Fe, Mg, Mn, K, Na) would affect the concentrations of the anthropogenic secondary inorganic aerosols. Fig. 21 depicts the seasonally averaged WBD impact on PSO4, PNO3 and PNH4 for 380 the ISORROPIA experiment.

Regarding sulphates, the strongest impacts occur during the winter reaching $0.1 \mu\text{gm}^{-3}$ over parts of Germany and Poland. In other seasons the impact remains less than $0.05 \mu\text{gm}^{-3}$ while it can be slightly negative in summer reaching $-0.01 \mu\text{gm}^{-3}$. PNO3 is shown to be increased with the presence of WBD too with values up to $0.1 \mu\text{gm}^{-3}$ in all seasons while most of the domain exhibit an increase above $0.01 \mu\text{gm}^{-3}$. Finally, PNH4 is decreased above the entire domain with values often exceeding 385 $-0.05 \mu\text{gm}^{-3}$ with peaking decreases around $-0.1 \mu\text{gm}^{-3}$ reached especially over the western part of the domain in winter.

The impact of WBD on secondary inorganic aerosol in the EQSAM experiments (Fig. 22) is evidently stronger in magnitude. The impact on PSO4 sometimes exceeds $0.1 \mu\text{gm}^{-3}$ and also the negative impact over Italy is stronger. In case of nitrates the impact also sometimes exceeds $0.1 \mu\text{gm}^{-3}$ and a larger area is marked with increase above $0.05 \mu\text{gm}^{-3}$ compared to the ISORROPIA. Finally, for ammonium, the decrease is larger than $0.01 \mu\text{gm}^{-3}$ and can exceed $0.1 \mu\text{gm}^{-3}$ being evidently 390 stronger than in the ISORROPIA experiment.

The geographical distribution of the seasonally averaged impact does not provide information about the possible daily extremes of the impacts of WBD on secondary aerosol. Therefore we also plotted the temporal evolution of the daily averaged change of PSO4, PNO3 and PNH4 concentrations due to WBD over the six selected urban areas.

Fig. 23 shows the WBD impact on the sulphates, while Fig. 24 and 25 shows the impact on nitrates and ammonium, 395 respectively.

In contrast with the seasonal low impact of WBD to the PSO4 concentrations, daily extreme values show an impact up to $0.5 \mu\text{gm}^{-3}$, while for some cities like Berlin even higher than $1 \mu\text{gm}^{-3}$. These usually occur during the cold part of the year in accordance with the spatial spatial results presented earlier. Daily WBD impact on nitrates is shown to be also higher than the seasonal one, with values reaching $1-1.5 \mu\text{gm}^{-3}$. The WBD impact on ammonium seems to have a decreasing effect, with 400 values ranging between -0.1 up to $-0.5 \mu\text{gm}^{-3}$, significantly higher than the seasonal ones as well.

4 Discussion and conclusions

This study ~~looked~~aimed at the potential long-term regional impact of dust emissions to PM2.5 and PM10 concentrations for the period 2007-2016. The analysis focused on Central Europe and on big urban areas such as Berlin, Prague, Vienna, Munich, Budapest and Warsaw. The impact was also estimated for the secondary inorganic aerosol concentrations as constituents of 405 PM2.5.

In our simulations, the annual average coarse and fine PM emitted averaged over the whole domain is about 1.5 and 0.5 $\text{Mg yr}^{-1} \text{km}^{-2}$, so about $2 \text{ Mg yr}^{-1} \text{km}^{-2}$ for the total PM10. This is by an order of higher value than calculated by Korcz et al. (2008) for Europe. The dust emissions show significant temporal and spatial patterns. Our dust model computed 2 times

stronger emissions during winter period than in summer (for both the fine and coarse dust particles). Over high latitude areas, 410 Bullard et al. (2016) reported strong winter dust emissions over areas where under dry conditions sublimation of snow (and eventually permafrost) occurs and the soil is more prone to saltation, while during summer, the soil is generally more moist reducing the saltation potential of soil particles. In the dust model used in this study, the three most important parameter affecting the dust emissions is the near-surface wind speed, snow equivalent water and soil moisture. The reason for much higher winter ~~wbdust~~ WBD emissions can be in 1) much higher winter windspeeds modelled compared to summer ones, lower 415 soil moisture during winter months and underestimation of snow cover which prevents dust events. We saw that our driving model (WRF) produced much higher winds than the measured ones and this positive bias is largest during winter. This strong overestimation is a known feature of the BouLac PBL scheme used in this study and others reported similar overestimation of wind speed (e.g. Tyagi et al., 2018; Zhang et al., 2021). As dust emissions scale non-linearly with wind speed that are above a threshold (Leung et al., 2022) this raises the potential to overestimate dust emissions if winds are overestimated. Our sensitivity 420 estimates confirmed this and even a @5% reduction of model wind-speeds greatly reduced the calculated WBD fluxes. We must note too that by driving WRF by the newer ERA-5 reanalysis data (Hersbach et al., 2017) instead of ERA-Interim some of the wind biases would be probably reduced as it shown by many (e.g .Belmonte Rivas and Stoffelen (2019)) that ERA-5 provides somewhat lower near-surface wind-speeds over Europe compared to ERA-Interim.

Regarding the modelled soil moisture, it is comparable to observed values in winter and somewhat higher during other 425 months than those measured. This means that the strong winter emissions are probably due to high wind-speeds in WRF. The last factor potentially playing a role is the snow cover which was not evaluated in this study, but the modelled precipitation exhibited some underestimation in winter which might result in reduced snow in our simulations (even though temperature is underestimated in winter).

Apart from the clear annual cycle, the calculated emissions show a diurnal cycle too. Daytime emissions are usually 50- 430 100% higher than nighttime ones. The reason for this is most probably due to the well-known cycle of wind-speed with maxima occurring during noon time ([Huszar et al., 2018, 2020](#)) ([Huszar et al., 2018, 2020](#)) and similar diurnal behaviour of dust emissions were seen in other studies too (e.g. Klose et al., 2012).

The daily timeseries of dust emissions provide some hint on their distribution: while most of the days, the coarse mode emissions remain low (lower than ~~10-20, which is about 100-200 0.1-0.2~~ $gs^{-1}km^{-2}$), on selected ~~day days~~ the emissions peak 435 at much higher values (~~100-200 of, i.e. 1000-2000 1-2~~ $gs^{-1}km^{-2}$). The same is true for the fine mode dust. This points to the fact already mentioned that the dust emissions respond non-linearly to wind speeds (more specifically to friction velocity, see Eq. 2) above a certain threshold. As wind speeds are overestimated in the driving meteorological model (WRF), probably the emissions are also overestimated, or at least these strong peaks are not realistic. Indeed, the sensitivity analysis to wind-speed reduction showed a very high sensitivity of WBD emissions on this parameter: making the wind-speeds half of the original values almost removed all WBD emissions. This means that very accurate meteorological driving data is needed to constrain the wind-blown dust emissions. We can further expect that due to the positive wind-bias and resulting overestimated WBD emissions, the actual dust emissions are closer to what Korcz et al. (2008) calculated.

One interesting feature is evident from the modelled geographical distribution of seasonal WBD emissions. Besides large 445 rural areas emitting dust, the largest dust sources are concentrated near large urban areas: the Ruhr area in Germany, the highly populated Benelux states, and also other large cities like Berlin, Prague, Budapest etc. One has to be very cautious in interpreting this result: dust is potentially emitted only over landuse categories representing potentially bare soil (if other circumstances are met), i.e. crops, shrubs, grass land, tundra and desert. "Urban" landuse is however not treated with dust emission potential. On the other hand, urban areas are ~~characterised~~characterized with low vegetation and thus leaf-area-index (LAI). Indeed, in the used LAI data (MODIS), cities have near zero LAI during most of the year. As landuse used for wbdust 450 module (and also for CAMx dry deposition) is represented as fractional landuse (based on CORINE data), many of the 9 km gridboxes covering urban areas are partly covered with bare soil and partly urban landuse. If the the LAI value is too low for such areas, the dust emission can occur in the model. This was the case for densely populated areas e.g. over the mentioned ~~Ruhr~~Ruhr area. In the case of large cities, as e.g. Berlin, dust emissions are concentrated near the edges of the city, where gridboxes share both urban landuse and ~~bair soil~~bare soil. ~~It is difficult to evaluate how realistic such "near" urban dust emissions are,~~ 455 ~~but~~Our sensitivity analysis on the way MODIS LAI is averaged over CAMx gridcells showed that if the lowest LAI values (assuming these constitute the urban fraction of the gridcell which cannot emit WBD) are omitted from the averaging, the resulting average LAI over the gridcell is much higher making the average WBD emissions smaller. Thus, this has to be treated as a cautious note on providing consistent input data for landuse and other land-related parameters like LAI with 460 preferably similar horizontal resolution.

Regarding the PM concentrations, the background noWBD case showed a reasonable model performance with typical correlations for PM2.5 and PM10 achieve in other modelling studies for Europe (e.g. Lecoer et al., 2013; Tsyro et al., 2022). Lowest correlations are computed for summer period while winter ones are usually the highest. This can be explained by the more stable weather conditions during DJF which are better resolved than summer weather often marked with highly variable convective environment (Huszar et al., 2016). The PM values are underestimated in summer and overestimated in winter which 465 is probably due to too strong vertical transport in summer and too low in winter, but may be connected also to deficiencies in the monthly profiles used for annual emissions (??)(Huszar et al., 2018, 2020). An important goal of the model validation was to evaluate whether the inclusion of WBD emission improves model performance. This turned out to be true for summer biases, which were reduced by adding the dust load. However, the winter which was already marked with negative bias, is modelled with even higher bias if dust is considered. Also the correlations decreased significantly if wind-blown dust is included in our 470 simulations. This can be explained by the strong peaks in the impact on PM values which are a result of strong emission peaks seen in the daily time series of FCRS and CCRS emissions. The modelled urban PM peaks are often much higher (often by a factor of 5 or even more) than measurements and thus can strongly reduce the correlation with the observed values. Also the RMSE values increased which can be again explained by the many outliers in the modelled PM data.

Similar to dust emissions, the WBD impact on overall PM concentrations is high near big urban centres (over Germany 475 and the Benelux states; reaching $15-20 \mu\text{gm}^{-3}$), but large rural contributions are modelled exceeding 2 and $5 \mu\text{gm}^{-3}$ too for PM2.5 and PM10, respectively. The contributions are largest, in accordance with the largest emissions , during winter and we seen a evident correlation of high concentrations of PM10 with high emissions of WBD in the coarse model. These seasonally

averaged impacts are however strongly exceeded by the daily average values which can be higher by 1 order of magnitude reaching $100 \mu\text{gm}^{-3}$ for some cities. However, as already said, these extreme peaks are probably overestimated (due to too strong winds in WRF).

Vautard et al. (2005) calculated the summer and autumn ~~wind-blow~~ wind-blown dust contribution to PM due to European local sources and found around $1\text{-}2 \mu\text{gm}^{-3}$ contribution to PM10 over central Europe which is about 2 times less than in our simulations. We can however expect that our result would get closer to their numbers without the positive wind-bias encountered in our driving model.

Apart from the impact on the overall PM2.5/10 concentrations, our study quantified the long-term impact on the aerosol secondary components, namely the secondary inorganic aerosol (SIA) components. In seasonal average, the impact are rather small, around up to $0.1 \mu\text{gm}^{-3}$ increase for PSO₄ (mainly during winter) and PNO₃ (all year round). For PNH₄, we modelled decreases of similar absolute magnitude. Much higher impact is however calculated for specific days as daily means. They can reach up to $0.5\text{-}1 \mu\text{gm}^{-3}$ increase for sulphates (maximum increase over Berlin in 2009 exceeding $1 \mu\text{gm}^{-3}$) and similar increases for nitrates. During winter 2008-2009, nitrates occasionally even decreased up to $0.2\text{-}0.3 \mu\text{gm}^{-3}$. Ammonium decreased due to dust by up to $-1 \mu\text{gm}^{-3}$ on selected days. These decreases occurred mainly during winter days.

The explanation of the above presented SIA modifications can be explained by two types of processes: one is the heterogeneous oxidation from SO₂ and N₂O₅ on the surface of dust particles (Wang et al., 2012; Zheng et al., 2015) and the other is the catalytic oxidation enhancement by dust elements in cloud water via influencing cloud pH and thus the aqueous chemistry of SO₂, HNO₃ and NH₃. Indeed, if we consider the impact of total SIA, we see that they increased (the increases of sulphates and nitrates overweight the decrease of ammonium). This is in line with the expectation and with previous studies dealing with the impact of dust on secondary aerosol formation (Malaguti et al., 2015).

Concretely, the increases of sulphates due to presence of dust particles were modelled by Wang et al. (2012) (increases by about $1 \mu\text{gm}^{-3}$ during a strong dust event in China) who attributed it to dust surface heterogeneous chemistry. Also Kakavas and Pandis (2021) modelled increases of sulphates over Europe due to dust. Our findings, at least qualitatively, are also in line with the recent findings of Wang et al. (2022) who argued that on the "dust surface, heterogeneous drivers are more efficient than surface-adsorbed oxidants in the conversion of SO₂, particularly during nighttime".

Regarding the impact on nitrates, the increases are consistent with an earlier study of Fairlie et al. (2010) who found that nitrates associate with dust and result in ~~volatilisation~~ volatilization. The increase of nitrates can be explained also by the formation of deliquescent salts (e.g., through the reaction of crustal cations in dust with NO³⁻ ions) as argued also by Wang et al. (2012). This can potentially lead to even some over-prediction of nitrates which requires the revisiting the chemical composition of dust (Karydis et al., 2011).

Finally, the ammonium response to dust is tightly connected to the response of sulphates and nitrates. As we saw that nitrates easily associate with dust (via reaction with dust crustal anions like Ca²⁺) this means that less nitrates is available to react with ammonium leading to more ammonia remaining in gas phase (Fairlie et al., 2010). In other words, NH₄⁺ is replaced by dust contained cations (Wang et al., 2012). This latest author and others (e.g. Malaguti et al., 2015) note that ammonium could

also increase due to dust presence as a result of more sulphates forming on dust surfaces. However, in our simulations this is evidently offset by the above mentioned replacement of ammonium by crustal cations.

515 In our experiments, the impact on SIA is clearly stronger using the EQSAM equilibrium model, although the differences are not large and the overall impact on PM is not affected too much. The reason for stronger sulphate and nitrate formation in EQSAM is probably due to the fact, that in EQSAM, the cloud pH is influenced with three cations (Mg^{++} , Ca^{++} and K^{+}) while in ISORROPIA, it is only Calcium. This also explains the stronger decrease of ammonium in EQSAM being replaced by more cations.

520 An exception of the above mentioned behaviour for nitrates is the winter 2009 decrease (by about $0.2 \mu\text{gm}^{-3}$) seen for all analysed cities. This period is not characterised by exceptional dust emissions nor extreme PM values (based on our results). On the other hand, during this period, the dust impact on PSO_4 is relatively large while the impact on ammonium is very small. Probably thus ammonium was neutralising preferably sulphates instead of nitrates causing their reduction.

525 Summing up the results, we showed that the long-term impact of local wind-blown dust emission in Europe can significantly enhance urban PM levels, especially during extreme events rather than in seasonal averages. However, our calculations are probably overestimating dust emissions due to very strong winds in the driving model. We also showed that apart from the total aerosol load, dust impacts also the secondary inorganic fraction of PM which can significantly increase during selected days.

530 We have to note also that the uncertainties related to different inputs used for the study cannot be well judged here. We already mentioned that the landuse and the LAI input can co-act (bare soil vs. low/high LAI) differently depending on the choice of these data. This caused for example that in our simulations one of the highest dust emissions are located around urban areas. We also used some default values for dust composition based on a study (Karydis et al., 2011) which measured this composition over a different geographic area. Lastly, we used only one driving model and one model for wind-blown dust emissions so the model uncertainty also cannot be addressed. The future goal should be thus to focus on the sensitivities of wind-blown dust loads to different input data and methods to obtain a more robust long-term estimate of their emissions and impact on PM and their secondary components.

535 *Data availability.* CAMx version 7.10 is available at <http://camx-wp.azurewebsites.net/download/source> (last access: 30 November 2022; CAMx, 2020; Ramboll et al., 2020). WRF version 4.0 can be downloaded from <https://www2.mmm.ucar.edu/wrf/src/WRFV4.0.TAR.gz> (last access 30 November 2022; WRF (2022)). The source code of the WBDUST model can be downloaded from the CAMx "Support Software" page: <https://www.camx.com/download/support-software/> (last access 30 November 2022; WBDUST (2022)). The LAI data used in WBDUST is obtained from <http://globalchange.bnu.edu.cn/research/laiv6> (Last access 30 November 2022; (Yuan et al., 2011)). The 540 complete model configuration and all the simulated data (three-dimensional hourly data) used for the analysis are stored at the Department of Atmospheric Physics, Charles University data storage facilities (about 5TB), and are available upon request from the main author. The observational data from the AirBase database can be obtained from <https://discomap.eea.europa.eu/map/fme/AirQualityExport.htm> (EEA, 2021). The data from the Czech Hydrometeorological Institute AIM network can be obtained upon request from the authors.

545 *Author contributions.* ML and PH conceptualized and designed the experiments and wrote the majority of the text, PH conducted the CAMx simulation, JK performed the WRF experiments, ML, LB, APPP contributed to the analysis of the results and OV helped with obtaining the observational data and writing the text.

Competing interests. No competing interests are present.

550 *Acknowledgements.* This work has been supported by the Czech Technological Agency (TACR) grant No.SS02030031 ARAMIS (Air Quality Research Assessment and Monitoring Integrated System) and Charles University Grant Agency (GAUK) project no. 298822. It has been partly funded also by the Austrian Climate and Energy Funds via project ACRP11-KR18AC0K14686 and the Charles University SVV 260581 project. We also further acknowledge the TNO-MACC-III emissions dataset provided by the Copernicus Monitoring Service, the compiled air quality station data provided by the European Environmental Agency, the ERA-Interim reanalysis provided by the European Centre for Medium-Range Weather Forecast, the MODIS leaf-area-data provided by Land-Atmosphere Interaction Research Group at Sun Yatsen University. We also thank the Czech Hydrometeorological Institute providing the AIM data.

555 **References**

Ansmann Albert, Jens Bösenberg, Anatoli Chaikovsky, Adolfo Comerón, Sabine Eckhardt, Ronald Eixmann, Volker Freudenthaler, Paul 560 Ginoux, Leonce Komguem, Holger Linné, Miguel Ángel López Márquez, Volker Matthias, Ina Mattis, Valentin Mitev, Detlef Müller, Svetlana Music, Slobodan Nickovic, Jacques Pelon, Laurent Sauvage, Piotr Sobolewsky, Manoj K. Srivastava, Andreas Stohl, Omar Torres, Geraint Vaughan, Ulla Wandinger, Matthias Wiegner: Long-range transport of Saharan dust to northern Europe: The 11–16 October 2001 outbreak observed with EARLINET, *J. Geophys. Res.*, 108(D24), 4783, <https://doi.org/10.1029/2003JD003757>, 2003

Astitha, M., Lelieveld, J., Abdel Kader, M., Pozzer, A. and de Meij, A.: Parameterization of dust emissions in the global atmospheric chemistry-climate model EMAC: impact of nudging and soil properties, *Atmos. Chem. Phys.*, 12, 11057–11083, <https://doi.org/10.5194/acp-12-11057-2012>, 2012.

[565 Belmonte Rivas, M. and Stoffelen, A.: Characterizing ERA-Interim and ERA5 surface wind biases using ASCAT, *Ocean Sci.*, 15, 831–852, <https://doi.org/10.5194/os-15-831-2019>, 2019.](#)

Benešová, N., Belda, M., Eben, K., Geletič, J., Huszár, P., Juruš, P., Krč, P., Resler, J. and Vlček, O.: New open source emission processor for air quality models, In Sokhi, R., Tiwari, P. R., Gállego, M. J., Craviotto Arnau, J. M., Castells Guiu, C. and Singh, V. (eds) Proceedings of Abstracts 11th International Conference on Air Quality Science and Application, doi: 10.18745/PB.19829. (pp. 27). Published by University of Hertfordshire. Paper presented at Air Quality 2018 conference, Barcelona, 12–16 March, 2018.

[570 Bessagnet, B., Menut, L., Aymoz, G., Chepfer, H., and Vautard, R.: Modelling dust emissions and transport within Europe: the Ukraine March 2007 event, *J. Geophys. Res.*, 113, D15202, <https://doi.org/10.1029/2007JD009541>, 2008.](#)

Birmili W., K. Schepanski, A. Ansmann, G. Spindler, I. Tegen, B. Wehner, A. Nowak, E. Reimer, I. Mattis, K. Muller, E. Brugge- 575 mann, T. Gnauk, H. Herrmann, A. Wiedensohler, D. Althausen, A. Schladitz, T. Tuch, and G. Loschau: A case of extreme particu- late matter concentrations over Central Europe caused by dust emitted over the southern Ukraine, *Atmos. Chem. Phys.*, 8, 997–1016, <https://doi.org/10.5194/acp-8-997-2008>, 2008

Bullard, J. E., Baddock, M., Bradwell, T., Crusius, J., Darlington, E., Gaiero, D., Gassó, S., Gisladottir, G., Hodgkins, R., McCulloch, R., McKenna-Neuman, C., Mockford, T., Stewart, H., and Thorsteinsson, T.: High-latitude dust in the Earth system, *Rev. Geophys.*, 54, 447–485, 2016.

Bougeault, P. and Lacarrère, P.: Parameterization of orography-induced turbulence in a meso-beta-scale model, *Mon. Weather Rev.*, 117, 580 1872–1890, 10.1175/1520-0493(1989)117<1872:POOITI>2.0.CO;2, 1989.

Byun, D. W. and Ching, J. K. S.: Science Algorithms of the EPA Model-3 Community Multiscale Air Quality (CMAQ) Modeling System, Office of Research and Development, U.S. EPA, North Carolina, EPA/600/R-99/030, 1999.

Buchholz, R. R., Emmons, L. K., Tilmes, S., and The CESM2 Development Team: CESM2.1/CAM-chem Instantaneous Output for Boundary 585 Conditions, UCAR/NCAR – Atmospheric Chemistry Observations and Modeling Laboratory, Subset used Lat: 10 to 80, Lon: 20 to 50, December 2014–January 2017, <https://doi.org/10.5065/NMP7-EP60>, 2019.

CAMx: Comprehensive Air Quality Model With Extensions version 7.10 code, Ramboll US Corporation, Novato, CA 94945, USA [code], <http://camx-wp.azurewebsites.net/download/source> (last access: 30 NOV 2022), 2020.

CORINE: CORINE Land Cover, European Union, Copernicus Land Monitoring Service 2012, European Environment Agency (EEA), <https://land.copernicus.eu/pan-european/corine-land-cover>, 2012.

[590 Chang, J.S., R.A. Brost, I.S.A. Isaksen, S. Madronich, P. Middleton, W.R. Stockwell, and C.J. Walcek: A Three-dimensional Eulerian Acid Deposition Model: Physical Concepts and Formulation. *J. Geophys. Res.*, 92, 14,681-14, 700, 1987.](#)

Chen, F. and Dudhia, J.: Coupling an Advanced Land Surface Hydrology Model with the Penn State-NCAR MM5 Modeling System. Part I: Model Implementation and Sensitivity, *Mon. Weather Rev.*, 129, [569–585](https://doi.org/10.1175/1520-0493(2001)129<0569:CAALSH>2.0.CO;2), [https://doi.org/10.1175/1520-0493\(2001\)129<0569:CAALSH>2.0.CO;2](https://doi.org/10.1175/1520-0493(2001)129<0569:CAALSH>2.0.CO;2), 2001.

595 Chen, S. and Sun, W.: A one-dimensional time dependent cloud model, *J. Meteorol. Soc. Jpn.*, 80, 99–118, <https://doi.org/10.2151/jmsj.80.99>, 2002.

Dorigo, W.A., Wagner, W., Albergel, C., Albrecht, F., Balsamo, G., Brocca, L., Chung, D., Ertl, M., Forkel, M., Gruber, A., Haas, E., Hamer, D. P. Hirschi, M., Ikonen, J., De Jeu, R. Kidd, R. Lahoz, W., Liu, Y.Y., Miralles, D., Lecomte, P. ESA CCI Soil Moisture for improved Earth system understanding: State-of-the art and future directions. In *Remote Sensing of Environment*, ISSN 0034-4257, 600 <https://doi.org/10.1016/j.rse.2017.07.001>, 2017

EEA: Air Quality e-Reporting products on EEA data service: E1a and E2a data sets, European Environment Agency, Copenhagen, Denmark [data set], <https://discomap.eea.europa.eu/map/fme/AirQualityExport.htm> (last access: 27 September 2022), 2021.

Emery, C., J. Jung, B. Koo, G. Yarwood.: Improvements to CAMx Snow Cover Treatments and Carbon Bond Chemical Mechanism for Winter Ozone. Prepared for the Utah Department of Environmental Quality, Division of Air Quality, Salt Lake City, UT. Prepared by 605 Ramboll Environ, Novato, CA, August, 2015.

Emmons, L. K., Schwantes, R. H., Orlando, J. J., Tyndall, G., Kinnison, D., Lamarque, J.-F., Marsh, D., Mills, M. J., Tilmes, S., Bardeen, Ch., Buchholz, R. R., Conley, A., Gettelman, A., Garcia, R., Simpson, I., Blake, D. R., Meinardi, S., and Pétron, G.: The Chemistry Mechanism in the Community Earth System Model version 2 (CESM2), *J. Adv. Model. Earth Sys.*, 12, e2019MS001882, <https://doi.org/10.1029/2019MS001882>, 2020.

610 Ramboll: User's Guide Comprehensive Air Quality Model With Extensions Version 7.10, User Guide, Ramboll US Corporation, Novato, CA 94945, USA, https://camx-wp.azurewebsites.net/Files/CAMxUsersGuide_v7.10.pdf (last access: 27 September 2022), 2020.

Fairlie D.T., Jacob D.J., Dibb J.E., Alexander B., Avery M.A., van Donkelaar A. , and Zhang L.: Impact of mineral dust on nitrate, sulfate, and ozone in transpacific Asian pollution plumes, *Atmos. Chem. Phys.*, 10, 3999–4012, doi:10.5194/acp-10-3999-2010, 2010

Fu X., Wang S., Chang X., Cai S., Xing J. and Hao J.: Modeling analysis of secondary inorganic aerosols over China: pollution characteristics, 615 and meteorological and dust impacts, *Nature Scientific Reports*, 6:35992, DOI: 10.1038/srep35992, 2016

Francis D., Fonseca R., Nellia N., Bozkurtbf D., BinGuande G.P.: Atmospheric rivers drive exceptional Saharan dust transport towards Europe, *Atm. Res.*, 266, 105959, <https://doi.org/10.1016/j.atmosres.2021.105959>, 2022

Giannadaki D., Pozzer A., and Lelieveld J.: Modeled global effects of airborne desert dust on air quality and premature mortality, *Atmos. Chem. Phys.*, 14, 957–968, <https://doi.org/10.5194/acp-14-957-2014>, 2014.

620 Global Multi-resolution Terrain Elevation Data 2010 (GMTED2010) Digital Object Identifier (DOI) number: /10.5066/F7J38R2N, 2010.

Grell, G.: Prognostic evaluation of assumptions used by cumulus parameterizations, *Mon. Weather Rev.*, 121, 764–787, [https://doi.org/10.1175/1520-0493\(1993\)121<0764:PEOAUB>2.0.CO;2](https://doi.org/10.1175/1520-0493(1993)121<0764:PEOAUB>2.0.CO;2), 1993.

Gruber, A., Scanlon, T., van der Schalie, R., Wagner, W., Dorigo, W.: Evolution of the CCI Soil Moisture Climate Data Records and their underlying merging methodology. *Earth System Science Data* 11, 717–739. <https://doi.org/10.5194/essd-11-717-2019>, 2019

625 Guenther, A. B., Jiang, X., Heald, C. L., Sakulyanontvittaya, T., Duhl, T., Emmons, L. K., and Wang, X.: The Model of Emissions of Gases and Aerosols from Nature version 2.1 (MEGAN2.1): an extended and updated framework for modeling biogenic emissions, *Geosci. Model Dev.*, 5, 1471–1492, <https://doi.org/10.5194/gmd-5-1471-2012>, 2012, 2012.

Gudmundsson L. and Seneviratne S.I.: Anthropogenic climate change affects meteorological drought risk in Europe, *Environ. Res. Lett.*, 11, 044005, doi:10.1088/1748-9326/11/4/044005, 2016.

630 [Hersbach, H., Bell, B., Berrisford, P., Hirahara, S., Horányi, A., MuñozSabater, J., Nicolas, J., Peubey, C., Radu, R., Schepers, D., Simmons, A., Soci, C., Abdalla, S., Abellan, X., Balsamo, G., Bechtold, P., Biavati, G., Bidlot, J., Bonavita, M., De Chiara, G., Dahlgren, P., Dee, D., Diamantakis, M., Dragani, R., Flemming, J., Forbes, R., Fuentes, M., Geer, A., Haimberger, L., Healy, S., Hogan, R.J., Hólm, E., Janisková, M., Keeley, S., Laloyaux, P., Lopez, P., Lupu, C., Radnoti, G., de Rosnay, P., Rozum, I., Vamborg, F., Villaume, S., Thépaut, J-N.: Complete ERA5 from 1979: Fifth generation of ECMWF atmospheric reanalyses of the global climate. Copernicus Climate Change Service \(C3S\) Data Store \(CDS\), 2017.](https://cds.climate.copernicus.eu/cdsapp#!/dataset/era5/reanalysis?view=dataset)

635 Huszár, P., Belda, M., and Halenka, T.: On the long-term impact of emissions from central European cities on regional air quality, *Atmos. Chem. Phys.*, 16, 1331-1352, doi:10.5194/acp-16-1331-2016, 2016.

Huszar, P., Belda, M., Karlický, J., Bardachova, T., Halenka, T., and Pisoft, P.: Impact of urban canopy meteorological forcing on aerosol concentrations, *Atmos. Chem. Phys.*, 18, 14059-14078, <https://doi.org/10.5194/acp-18-14059-2018>, 2018.

640 Huszar, P., Karlický, J., Ďoubalová, J., Šindelářová, K., Nováková, T., Belda, M., Halenka, T., Žák, M., and Pišoft, P.: Urban canopy meteorological forcing and its impact on ozone and PM2.5: role of vertical turbulent transport, *Atmos. Chem. Phys.*, 20, 1977–2016, <https://doi.org/10.5194/acp-20-1977-2020>, 2020.

Iacono, M. J., Delamere, J. S., Mlawer, E. J., Shephard, M. W., Clough, S. A., and Collins, W. D.: Radiative forcing by long-lived greenhouse gases: Calculations with the aer radiative transfer models. *Journal of Geophysical Research: Atmospheres*, 113 (D13103).
645 <http://dx.doi.org/10.1029/2008JD009944>, 2008.

Janjic, Z. I.: The step-mountain eta coordinate model: Further developments of the 172 convection, viscous sublayer, and turbulence closure schemes. *Monthly Weather Re173 view*, 122 (5), 927-945, [https://doi.org/10.1175/1520-0493\(1994\)122<0927:TSMECM>2.0.CO;2](https://doi.org/10.1175/1520-0493(1994)122<0927:TSMECM>2.0.CO;2), 1994.

Kakavas, S. and Pandis, S. N.: Effects of urban dust emissions on fine and coarse PM levels and composition, *Atmos. Environ.*, 246, 118006, 650 <https://doi.org/10.1016/j.atmosenv.2020.118006.>, 2021.

Karlický, J., Huszár, P., Halenka, T., Belda, M., Žák, M., Pišoft, P., and Mikšovský, J.: Multi-model comparison of urban heat island modelling approaches, *Atmos. Chem. Phys.*, 18, 10655–10674, <https://doi.org/10.5194/acp-18-10655-2018>, 2018.

Karlický, J., Huszár, P., Nováková, T., Belda, M., Švábik, F., Ďoubalová, J., and Halenka, T.: The “urban meteorology island”: a multi-model ensemble analysis, *Atmos. Chem. Phys.*, 20, 15061–15077, <https://doi.org/10.5194/acp-20-15061-2020>, 2020.

655 Karydis, V. A., Tsimpidi, A. P., Lei, W., Molina, L. T., and Pandis, S. N.: Formation of semivolatile inorganic aerosols in the Mexico City Metropolitan Area during the MILAGRO campaign, *Atmos. Chem. Phys.*, 11, 13305–13323, <https://doi.org/10.5194/acp-11-13305-2011>, 2011.

Keet A. Corinne, Keller P. Joshua, and Peng D. Roger: Long-Term Coarse Particulate Matter Exposure Is Associated with Asthma among Children in Medicaid, *Am. J. Respir. Crit. Care Med.* 197, 737-746, <https://doi.org/10.1164/rccm.201706-1267OC>, 2018.

660 Klingmüller, K., Metzger, Abdelkader, M., Karydis, V. A., Stenchikov, G. L., Pozzer, A., and Lelieveld, J.: Revised mineral dust emissions in the atmospheric chemistry-climate model EMAC (MESSy 2.52 DU_Astitha1 KKDU2017 patch), *Geosci. Model Dev.*, 11: 989–1008, <https://doi.org/10.5194/gmd-11-989-2018>, 2018.

Klose, M. and Shao, Y.: Stochastic parameterization of dust emission and application to convective atmospheric conditions, *Atmos. Chem. Phys.*, 12, 7309–7320, <https://doi.org/10.5194/acp-12-7309-2012>, 2012.

665 Korcz, M., Fudała, J. and Kliś, Cz.: Estimation of wind blown dust emissions in Europe and its vicinity, *Atmospheric Environment*, 43, Issue 7, 1410-1420, <https://doi.org/10.1016/j.atmosenv.2008.05.027>, 2008.

Kuenen, J. J. P., Visschedijk, A. J. H., Jozwicka, M., and Denier van der Gon, H. A. C.: TNO-MACC_II emission inventory; a multi-year (2003–2009) consistent high-resolution European emission inventory for air quality modelling, *Atmos. Chem. Phys.*, 14, 10963–10976, <https://doi.org/10.5194/acp-14-10963-2014>, 2014.

670 Kusaka, H., Kondo, K., Kikegawa, Y., and Kimura, F.: A simple single-layer urban canopy model for atmospheric models: Comparison with multi-layer and slab models, *Bound.-Lay. Meteorol.*, 101, 329–358, 2001.

Lecoer, È. and Seigneur, C.: Dynamic evaluation of a multi-year model simulation of particulate matter concentrations over Europe, *Atmos. Chem. Phys.*, 13, 4319–4337, <https://doi.org/10.5194/acp-13-4319-2013>, 2013.

675 Leung, D. M., Kok, J. F., Li, L., Okin, G. S., Prigent, C., Klose, M., Garcia-Pando, C. P., Menut, L., Mahowald, N. M., Lawrence, D. M., and Chamecki, M.: A new process-based and scale-respecting desert dust emission scheme for global climate models – Part I: description and evaluation against inverse modeling emissions, *Atmos. Chem. Phys. Discuss. [preprint]*, <https://doi.org/10.5194/acp-2022-719>, in review, 2022.

680 Malaguti A, Mircea M., La Torretta T. M.G., Telloli C., Petralia E., Stracquadanio M., Berico M.: Chemical Composition of Fine and Coarse Aerosol Particles in the Central Mediterranean Area during Dust and Non-Dust Conditions, *Aerosol and Air Quality Research*, 15: 410–425, doi: 10.4209/aaqr.2014.08.0172, 2015.

Meinander, O., Dagsson-Waldhauserova, P., Amosov, P., Aseyeva, E., Atkins, C., Baklanov, A., Baldo, C., Barr, S. L., Barzycka, B., Benning, L. G., Cvetkovic, B., Enchilik, P., Frolov, D., Gassó, S., Kandler, K., Kasimov, N., Kavan, J., King, J., Koroleva, T., Krupskaya, V., Kulmala, M., Kusiak, M., Lappalainen, H. K., Laska, M., Lasne, J., Lewandowski, M., Luks, B., McQuaid, J. B., Moroni, B., Murray, B., Möhler, O., Nawrot, A., Nickovic, S., O'Neill, N. T., Pejanovic, G., Popovicheva, O., Ranjbar, K., Romanias, M., Samonova, O., Sanchez-685 Marroquin, A., Schepanski, K., Semenkov, I., Sharapova, A., Shevrina, E., Shi, Z., Sofiev, M., Thevenet, F., Thorsteinsson, T., Timofeev, M., Umo, N. S., Uppstu, A., Urupina, D., Varga, G., Werner, T., Arnalds, O., and Vukovic Vimic, A.: Newly identified climatically and environmentally significant high-latitude dust sources, *Atmos. Chem. Phys.*, 22, 11889–11930, <https://doi.org/10.5194/acp-22-11889-2022>, 2022.,

690 Metzger, S., Steil, B., Abdelkader, M., Klingmüller, K., Xu, L., Penner, J. E., Fountoukis, C., Nenes, A., and Lelieveld, J.: Aerosol water parameterisation: a single parameter framework, *Atmos. Chem. Phys.*, 16, 7213–7237, <https://doi.org/10.5194/acp-16-7213-2016>, 2016.

Nenes, A. C. Pilinis, and S.N. Pandis: ISORROPIA: A New Thermodynamic Model for Multiphase Multicomponent Inorganic Aerosols. *Aquatic Geochemistry*, 4, 123–152, <https://doi.org/10.1023/A:1009604003981>, 1998.

695 Nenes, A., C. Pilinis, and S.N. Pandis: Continued Development and Testing of a New Thermodynamic Aerosol Module for Urban and Regional Air Quality Models. *Atmos. Environ.* 33, 1553–1560., 10.1016/S1352-2310%2898%2900352-5, 1999.

Passant, N.: Speciation of UK Emissions of Non-methane Volatile Organic Compounds, DEFRA, AEAT/ENV/R/0545 Issue 1, 2002.

Ryder C. L., E. J. Highwood, P. D. Rosenberg, J. Trembath, J. K. Brooke, M. Bart, A. Dean3, J. Crosier, J. Dorsey, H. Brindley, J. Banks, J. H. Marsham, J. B. McQuaid, H. Sodemann, and R. Washington: Optical properties of Saharan dust aerosol and contribution from the coarse mode as measured during the Fennec 2011 aircraft campaign, *Atmos. Chem. Phys.*, 13, 303–325, <https://doi.org/10.5194/acp-13-303-2013>, 2013.

700 Shangguan, W., Dai, Y., Duan, Q., Liu, B. and Yuan, H.: A global soil data set for earth system modeling, *J. Adv. Model. Earth Syst.*, 6, 249–263, doi:10.1002/2013MS000293., 2014.

Simmons, A. J., Willett, K. M., Jones, P. D., Thorne, P. W., and Dee, D. P.: Low-frequency variations in surface atmospheric humidity, temperature and precipitation: inferences from reanalyses and monthly gridded observational datasets, *J. Geophys. Res.*, 115, D01110, doi:10.1029/2009JD012442, 2010.

705 Sindelarova, K., Granier, C., Bouarar, I., Guenther, A., Tilmes, S., Stavrakou, T., Müller, J.-F., Kuhn, U., Stefani, P., and Knorr, W.: Global data set of biogenic VOC emissions calculated by the MEGAN model over the last 30 years, *Atmos. Chem. Phys.*, 14, 9317–9341, <https://doi.org/10.5194/acp-14-9317-2014>, 2014.

Skamarock, W. C., J. B. Klemp, J. Dudhia, D. O. Gill, Z. Liu, J. Berner, W. Wang, J. G. Powers, M. G. Duda, D. M. Barker, and X.-Y. Huang: A Description of the Advanced Research WRF Version 4. NCAR Tech. Note NCAR/TN-556+STR, 145 pp. doi:10.5065/1dfh-6p97, 2019.

710 Song, Q., Zhang, Z., Yu, H., Kok, J. F., Di Biagio, C., Albani, S., Zheng, J., and Ding, J.: Size-resolved dust direct radiative effect efficiency derived from satellite observations, *Atmos. Chem. Phys.*, 22, 13115–13135, <https://doi.org/10.5194/acp-22-13115-2022>, 2022.

Stagge J.H., Kingston D.G., Tallaksen L.M., David M. H.: Observed drought indices show increasing divergence across Europe, *Sci Rep* 7, 14045, <https://doi.org/10.1038/s41598-017-14283-2>, 2017.

715 Strader, R., F. Lurmann and S.N. Pandis: Evaluation of secondary organic aerosol formation in winter. *Atmos. Environ.*, 33, 4849–4863, 1999.

Tsyro, S., Aas, W., Colette, A., Andersson, C., Bessagnet, B., Ciarelli, G., Couvidat, F., Cuvelier, K., Manders, A., Mar, K., Mircea, M., Otero, N., Pay, M.-T., Raffort, V., Roustan, Y., Theobald, M. R., Vivanco, M. G., Fagerli, H., Wind, P., Briganti, G., Cappelletti, A., D'Isidoro, M., and Adani, M.: Eurodelta multi-model simulated and observed particulate matter trends in Europe in the period of 1990–2010, *Atmos. Chem. Phys.*, 22, 7207–7257, <https://doi.org/10.5194/acp-22-7207-2022>, 2022.

720 Tyagi, B.; Magliulo, V.; Finardi, S.; Gasbarra, D.; Carlucci, P.; Toscano, P.; Zaldei, A.; Riccio, A.; Calori, G.; D'Allura, A.; Gioli, B. Performance Analysis of Planetary Boundary Layer Parameterization Schemes in WRF Modeling Set Up over Southern Italy. *Atmosphere*, 9, 272. <https://doi.org/10.3390/atmos9070272>, 2018.

van der Gon, H. D., Hendriks, C., Kuenen, J., Segers, A. and Visschedijk, A.: Description of current temporal emission patterns and sensitivity of predicted AQ for temporal emission patterns. EU FP7 MACC deliverable report D_D-EMIS_1.3, http://www.gmes-atmosphere.eu/documents/deliverables/d-emis/MACC_TNO_del_1_3_v2.pdf, 2011.

725 Vautard, R., B. Bessagnet, M. Chin, and L. Menut: On the contribution of natural aeolian sources to particulate matter concentrations in Europe: Testing hypotheses with a modelling approach, *Atmos. Environ.*, 39, 3291–3303., 2005.

Wagner, R., Jähn Michael, and Schepanski Kerstin: Wildfires as a source of airborne mineral dust – revisiting a conceptual model using large-eddy simulation (LES), *Atmos. Chem. Phys.*, 18, 11863–11884, <https://doi.org/10.5194/acp-18-11863-2018>, 2018.

730 Wang, K., Zhang, Y., Nenes, A., and Fountoukis, C.: Implementation of dust emission and chemistry into the Community Multi-scale Air Quality modeling system and initial application to an Asian dust storm episode, *Atmos. Chem. Phys.*, 12, 10209–10237, <https://doi.org/10.5194/acp-12-10209-2012>, 2012.

Wang Q., Gub J., Wang X.: The impact of Sahara dust on air quality and public health in European countries, *Atmos. Env.*, 241, 117771, <https://doi.org/10.1016/j.atmosenv.2020.117771>, 2020.

735 Wang, T., Liu, Y., Cheng, H., Wang, Z., Fu, H., Chen, J., and Zhang, L.: Significant formation of sulfate aerosols contributed by the heterogeneous drivers of dust surface, *Atmos. Chem. Phys.*, 22, 13467–13493, <https://doi.org/10.5194/acp-22-13467-2022>, 2022.

WBDUST[code]: [Wind-blow](#) [Wind-blown](#) dust module code, <https://www.camx.com/download/support-software/> (last access 30 November 2022), 2022.

740 WRF[code]: Weather Research and Forecast model code, version 4.0 source code, <https://www2.mmm.ucar.edu/wrf/src/WRFV4.0.TAR.gz> (last access 30 November 2022), 2022.

Yang, L., Mickley J. Loretta, Kaplan O. Jed: Response of dust emissions in southwestern North America to 21st century trends in climate, CO₂ fertilization, and land use: Implications for air quality, *Atmos. Chem. Phys.*, 21(1):57-68, <https://doi.org/10.5194/acp-2020-311>, 2021.

Yarwood, G., J. Jung, G. Z. Whitten, G. Heo, J. Mellberg and E. Estes. 2010. Updates to the Carbon Bond Mechanism for Version 6 (CB6).
745 Presented at the 9th Annual CMAS Conference, Chapel Hill, October, 2010.

Yuan, H., Dai, Y., Xiao, Z., Ji, D., Shangguan, W.: Reprocessing the MODIS Leaf Area Index Products for Land Surface and Climate Modelling. *Remote Sensing of Environment*, 115(5), 1171-1187. doi:10.1016/j.rse.2011.01.001, 2011.

Zhang, L.; Xin, J.; Yin, Y.; Chang, W.; Xue, M.; Jia, D.; Ma, Y. Understanding the Major Impact of Planetary Boundary Layer Schemes on Simulation of Vertical Wind Structure. *Atmosphere*, 12, 777. , 2021.

750 Zheng, B., Zhang, Q., Zhang, Y., He, K. B., Wang, K., Zheng, G. J., Duan, F. K., Ma, Y. L., and Kimoto, T.: Heterogeneous chemistry: a mechanism missing in current models to explain secondary inorganic aerosol formation during the January 2013 haze episode in North China, *Atmos. Chem. Phys.*, 15, 2031–2049, <https://doi.org/10.5194/acp-15-2031-2015>, 2015.

Zittis, G., Almazroui, M., Alpert, P., Ciais, P., Cramer, W., Dahdal, Y., et al.: Climate change and weather extremes in the Eastern Mediterranean and Middle East. *Rev. Geophys.* 60, e2021RG000762. doi:10.1029/2021RG000762, 2022.

755 Zwaafink G., C. D., Aas, W., Eckhardt, S., Evangelou, N., Hamer, P., Johnsrud, M., Kylling, A., Platt, S. M., Stebel, K., Uggerud, H., and Yttri, K. E.: What caused a record high PM10 episode in northern Europe in October 2020?, *Atmos. Chem. Phys.*, 22, 3789–3810, <https://doi.org/10.5194/acp-22-3789-2022>, 2022.

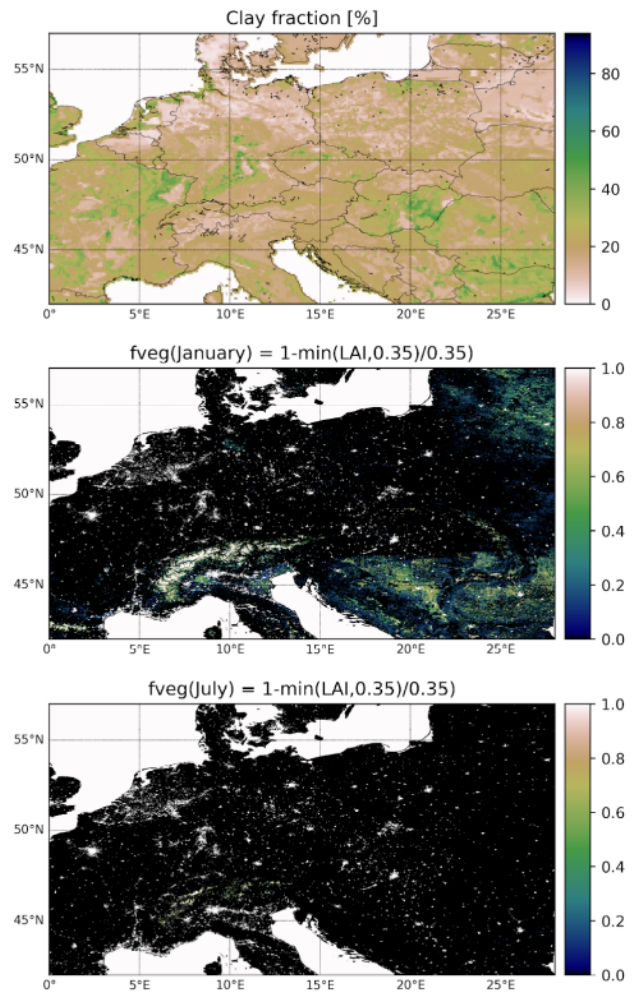


Figure 1. The input data for the clay fraction in % (top) and the vegetation factor for January and July (middle and bottom, respectively) based on MODIS 2010 LAI data

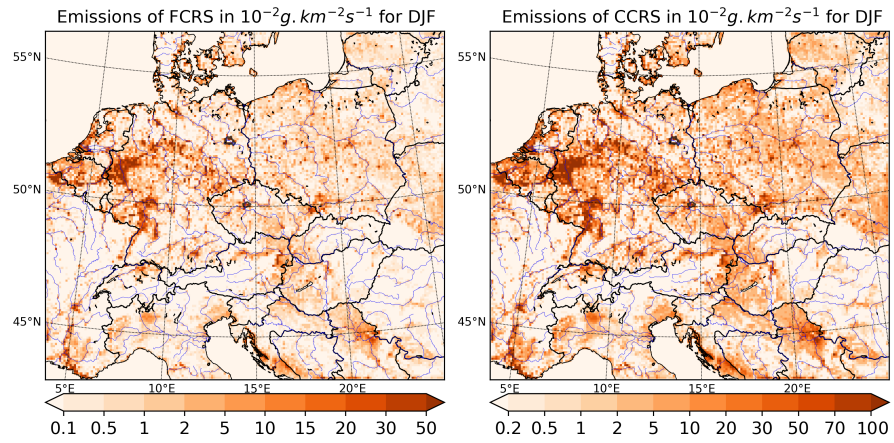


Figure 2. Average seasonal WBD emission fluxes of Fine Crustal material (FCRS; left) and of Coarse Crustal material (CCRS; right) above central Europe in DJF for 2007-2016 period in $10^{-2} \text{gs}^{-1} \text{km}^{-2}$. Note that the colorbars are different.

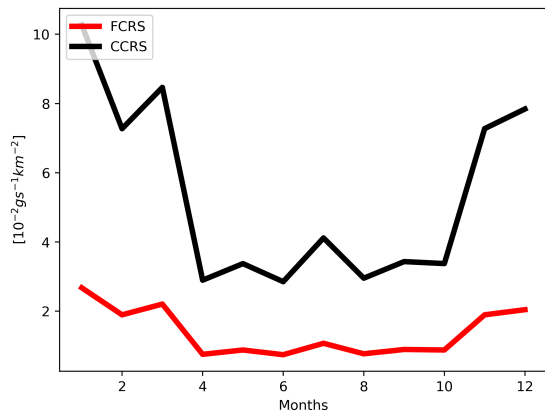


Figure 3. Domain-averaged annual cycle of monthly averages of FCRS and CCRS WBD emission fluxes for 2007-2016 in $10^{-2} \text{gs}^{-1} \text{km}^{-2}$.

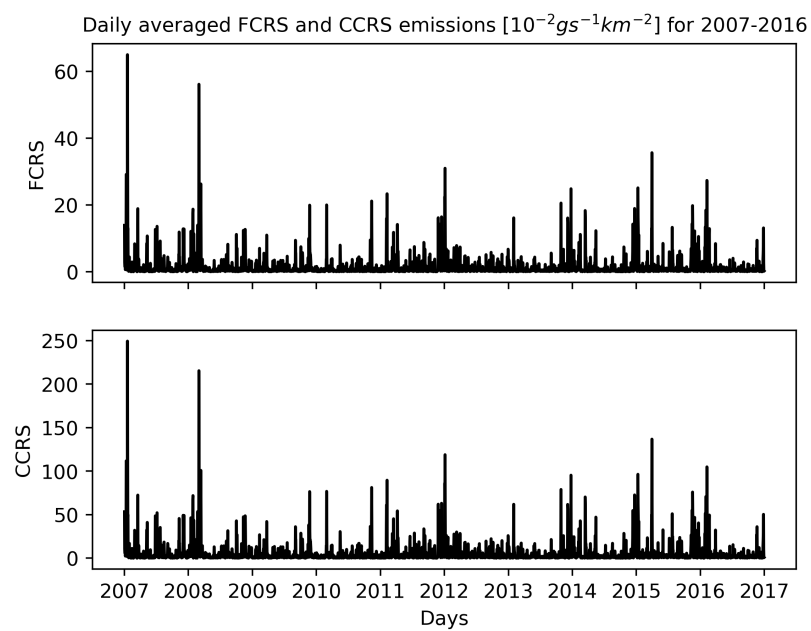


Figure 4. Domain-averaged daily WBD emission fluxes of FCRS (top) and CCRS (bottom) for 2007-2016 in $10^{-2} \text{gs}^{-1} \text{km}^{-2}$.

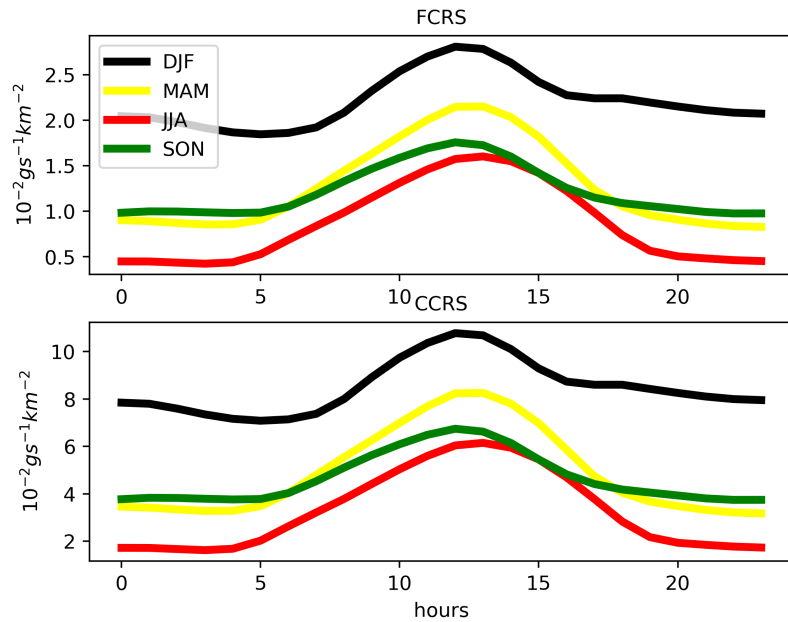


Figure 5. Domain-averaged diurnal cycle of hourly FCRS and CCRS WBD emission fluxes for different seasons [in-for](#) 2007-2016. Units in $10^{-2} \text{gs}^{-1} \text{km}^{-2}$.

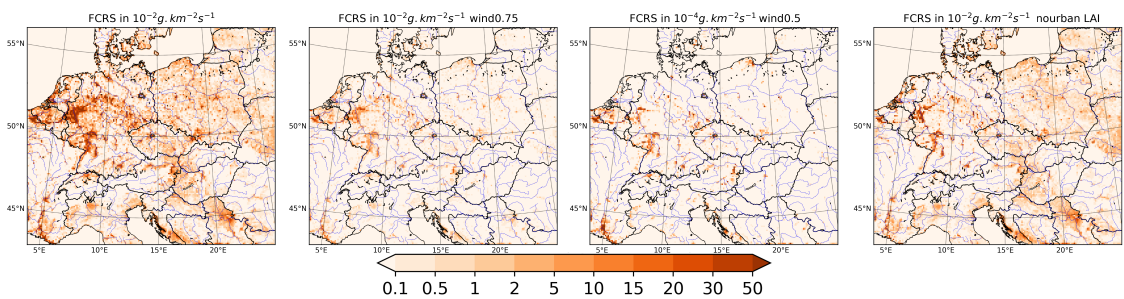


Figure 6. Average WBD emission fluxes of Fine Crustal material (FCRS) above central Europe in DJF for 2007-2016. From left to right: the default WBD emissions, WBD emissions after 0.75x reduction of wind-speeds, WBD emissions after 0.5x reduction of wind-speeds, emissions with LAI averaged only over non-urban gridcell fractions. Note that the units for 0.5 wind reduction have an order of 10^{-4} while 10^{-2} for the rest.

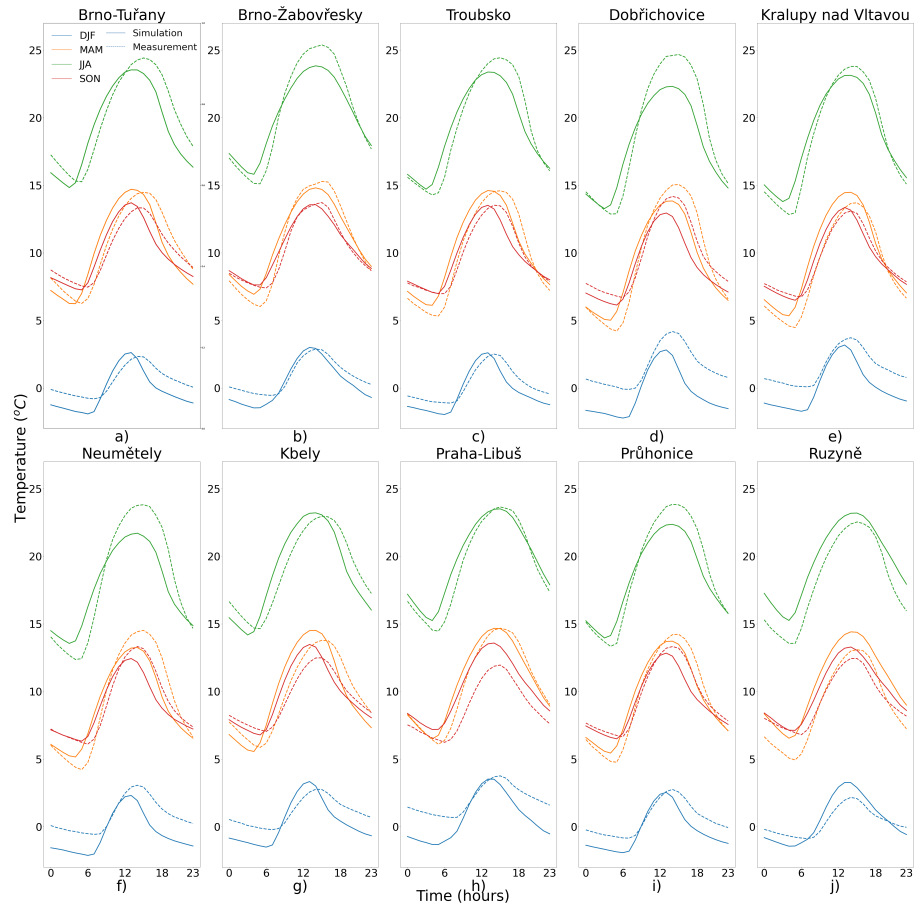


Figure 7. Comparison of modelled temperature diurnal profiles (solid) with measurements (dashed) from 10 Czech stations averaged over different seasons for the 2007-2016 period. Units in $^{\circ}\text{C}$

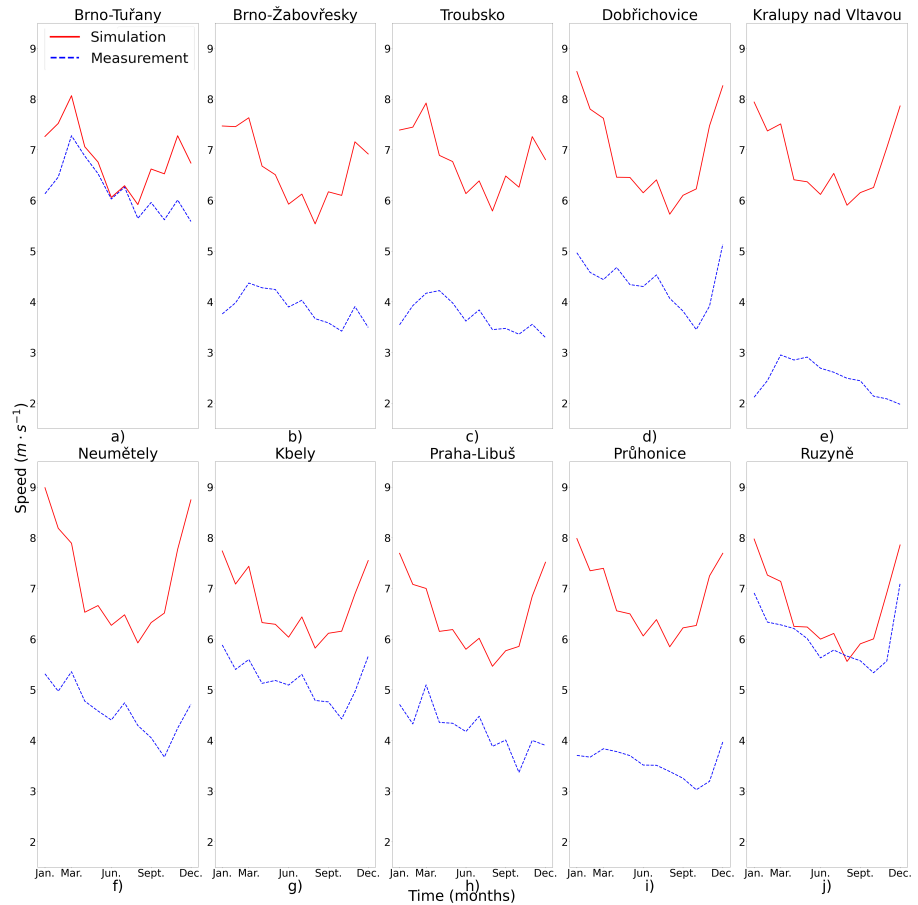


Figure 8. Comparison of modelled annual cycle of the monthly mean of maximum daily wind-speeds (red solid) with measurements (blue dashed) from 10 Czech stations averaged over the 2007-2016 period. Units in ms^{-1}

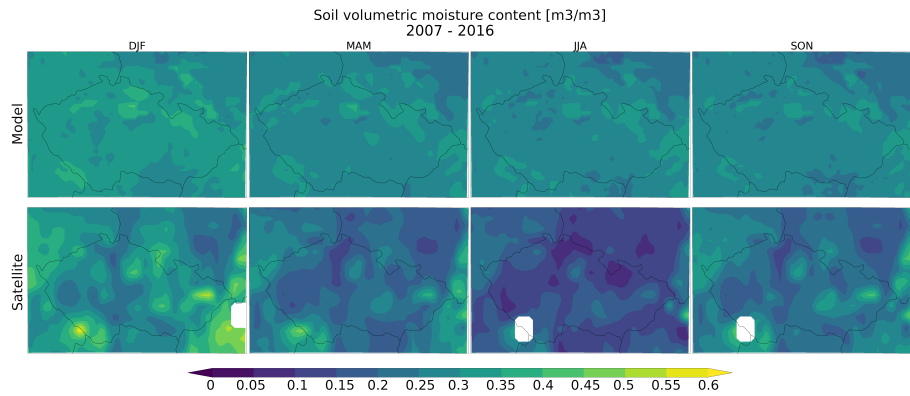


Figure 9. Comparison of modelled seasonal volumetric soil moisture (upper row) with the ESA CCI soil moisture data (lower row) for the area of Czech republic. Data averaged over 2007-2016. Units in $\text{m}^3 \text{m}^{-3}$.

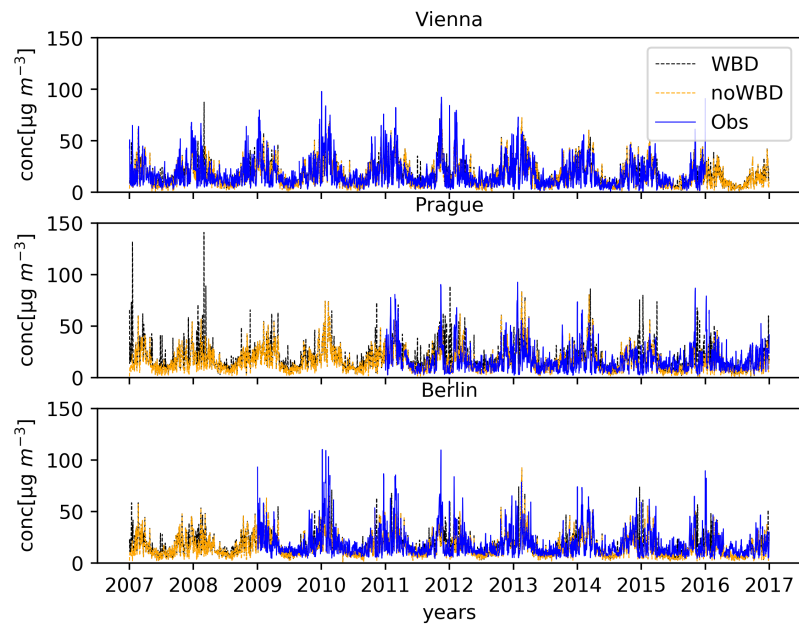


Figure 10. PM2.5 daily averaged concentrations of WBD (black dashed), noWBD (orange dashed) and Airbase dataset (blue solid) for 2007-2016 (Vienna, Prague, Berlin). Units in μgm^{-3} .

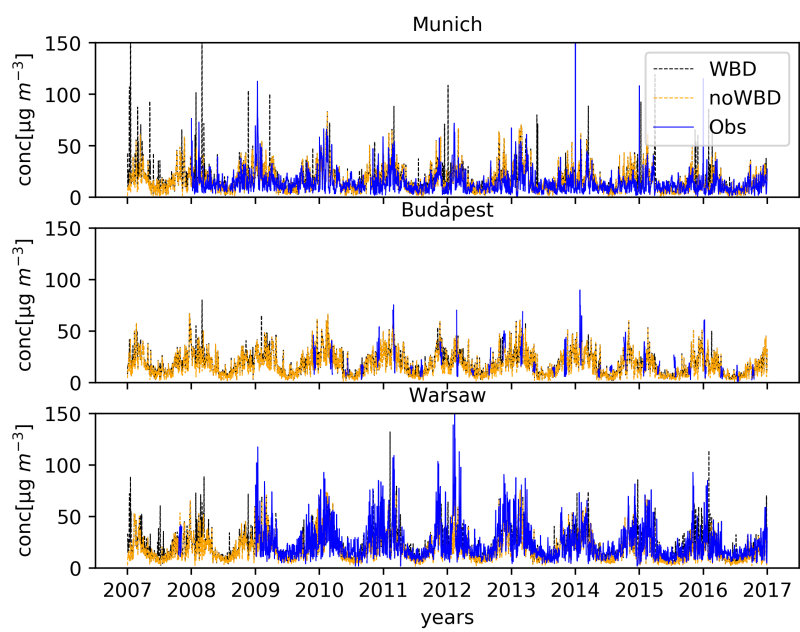


Figure 11. Same as Fig 12 but for Munich, Budapest, Warsaw.

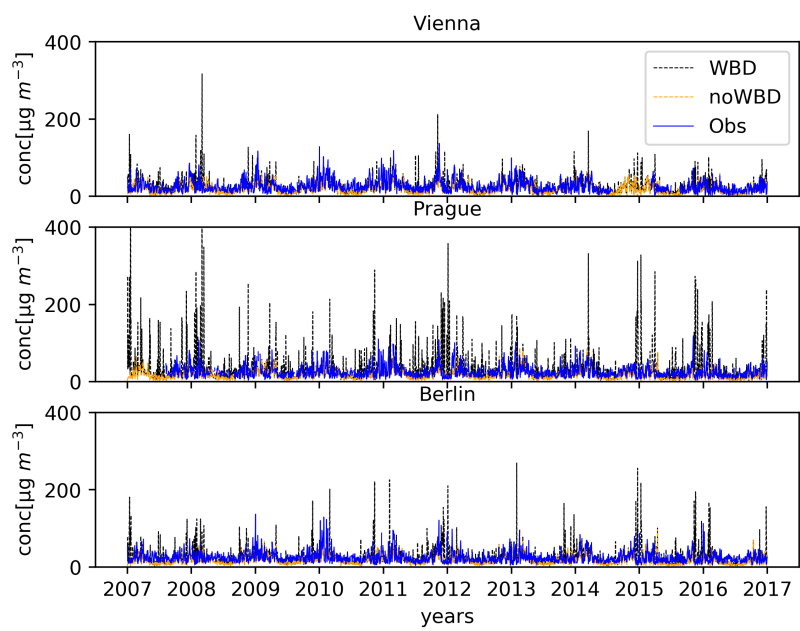


Figure 12. PM10 daily averaged concentrations of WBD (black dashed), noWBD (orange dashed) and Airbase dataset (blue solid) for 2007-2016 (Vienna, Prague, Berlin). Units in $\mu\text{g m}^{-3}$.

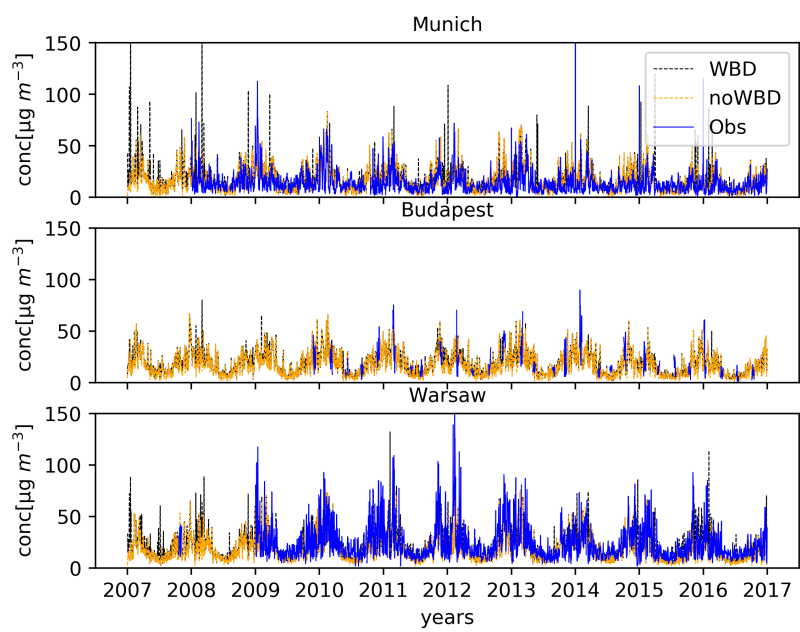


Figure 13. Same as Fig 12 but for Munich, Budapest, Warsaw.

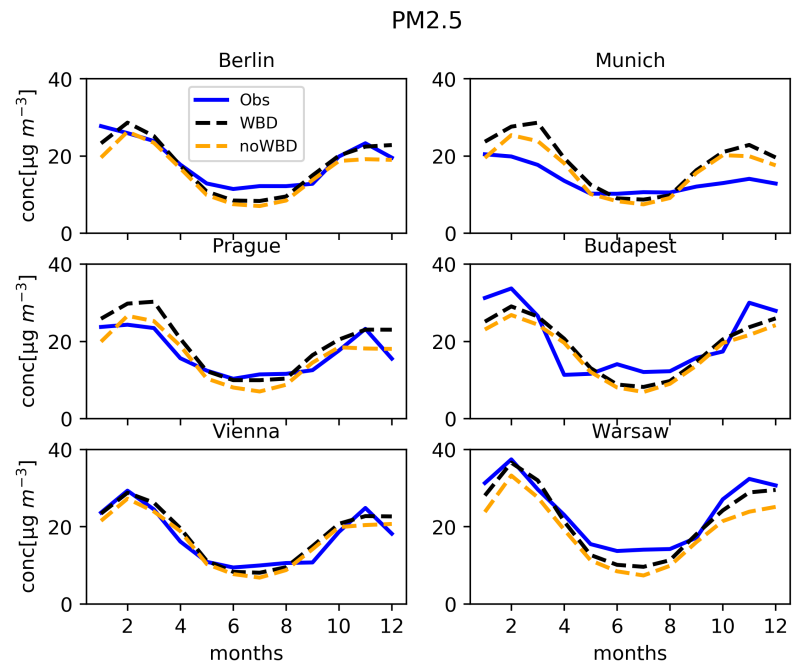


Figure 14. Annual cycle of monthly PM2.5 concentrations of WBD (blue dashed), noWBD (orange dashed) simulations and Airbase dataset (blue solid) for 2007-2016.

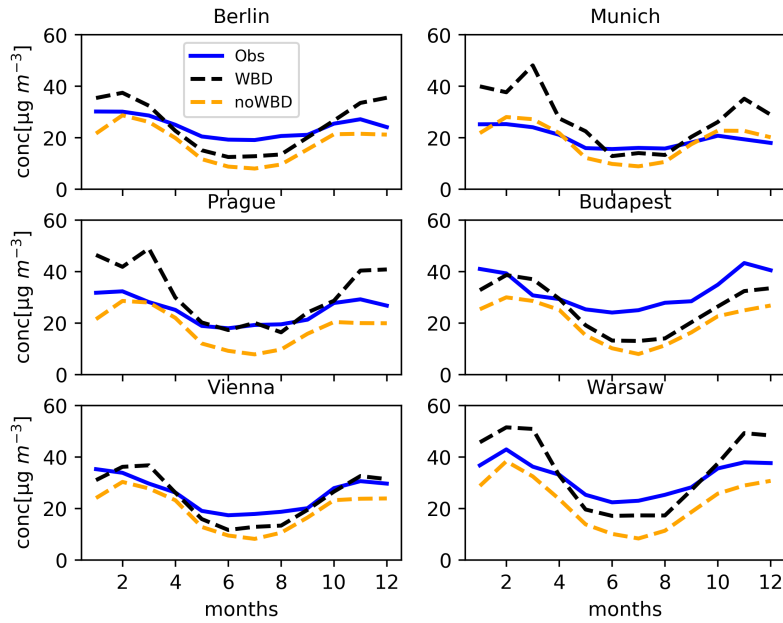


Figure 15. Annual cycle of monthly PM10 concentrations of WBD (blue dashed), noWBD (orange dashed) simulations and Airbase dataset (blue solid) for 2007-2016.

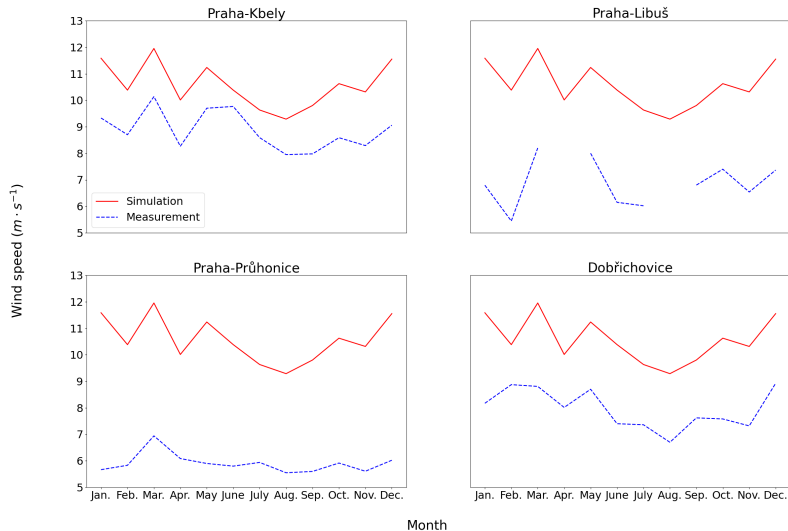


Figure 16. Annual cycle of monthly averaged maximum daily wind-speeds from model simulation (red) and observations from four station in/around Prague (red); averaging is done for days when the daily PM10 model bias is larger than $50 \mu\text{g m}^{-3}$.

Impact of WBD emissions on urban PM2.5 concentrations

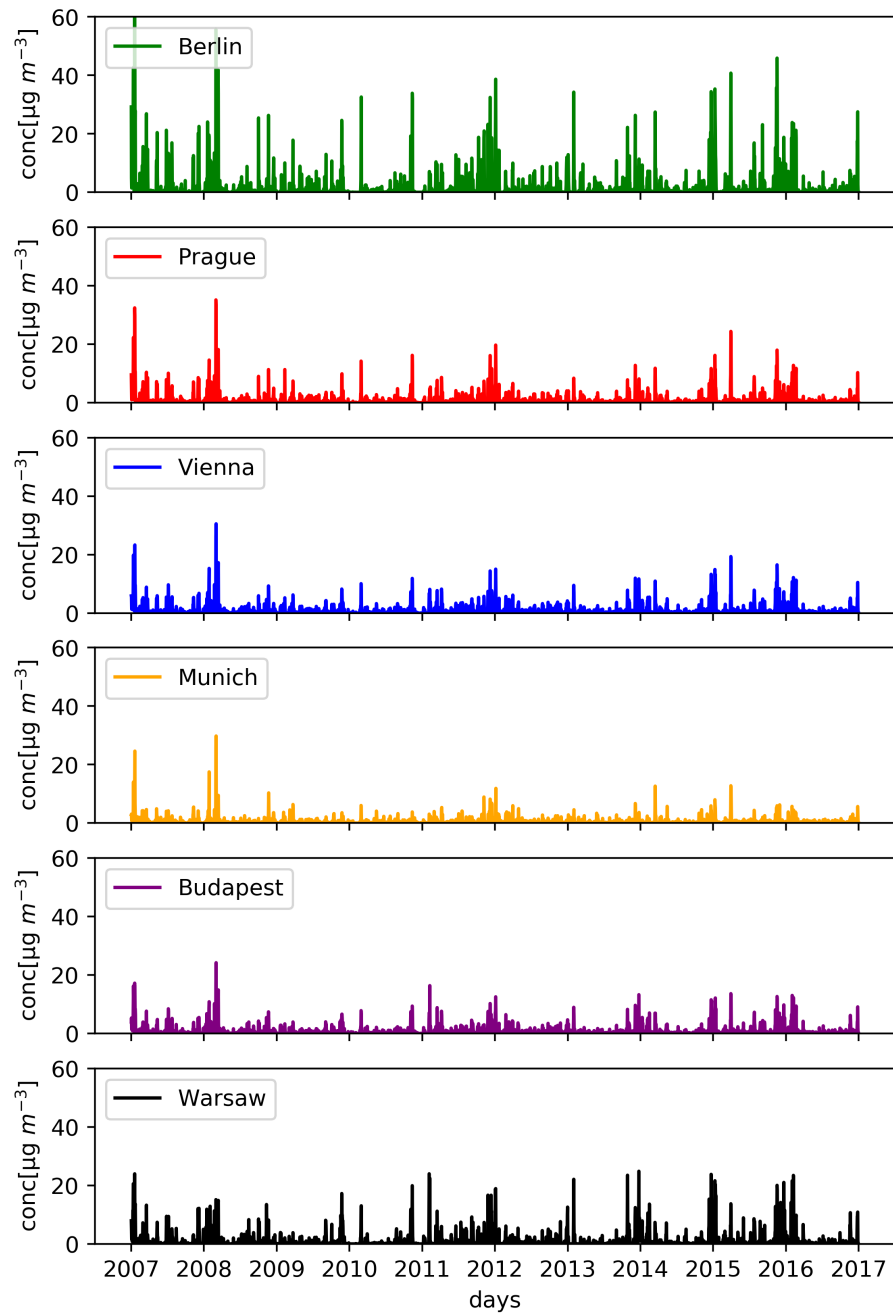


Figure 17. Daily averaged impact of wind-blown dust emissions on PM2.5 concentrations in $\mu\text{g m}^{-3}$ for 2007-2016.

Impact of WBD emissions on urban PM10 concentrations

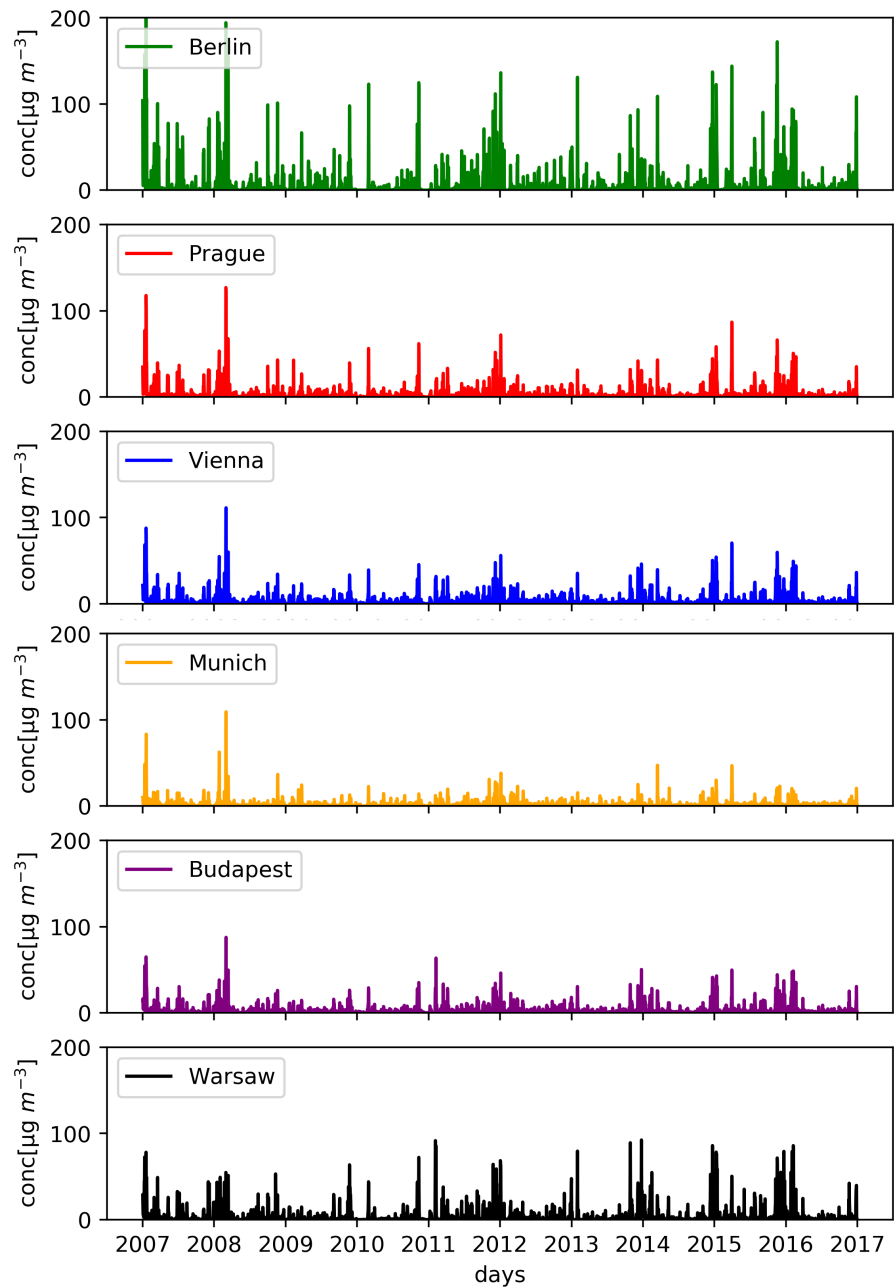


Figure 18. Daily averaged impact of wind-blown dust emissions on PM10 concentrations in $\mu\text{g m}^{-3}$ for 2007-2016.

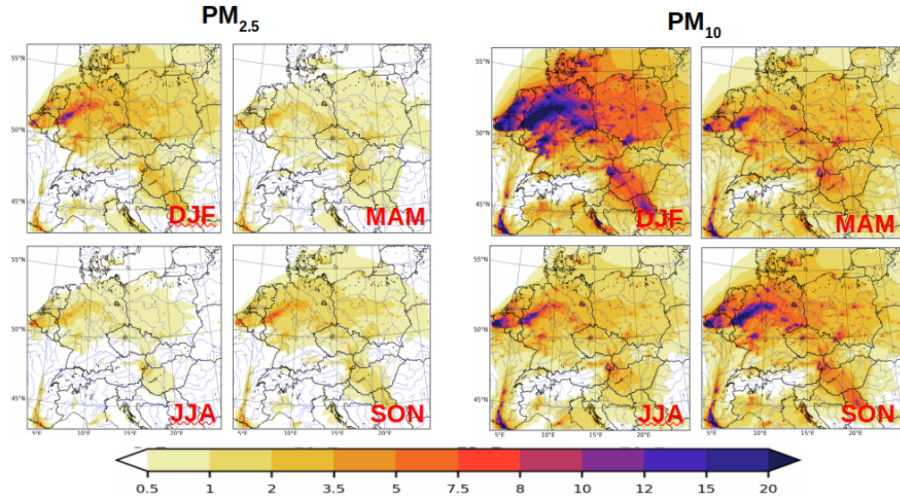


Figure 19. Seasonally averaged impact of WBD emissions to PM2.5 (left) and PM10 (right) concentrations in μgm^{-3} for 2007-2016.

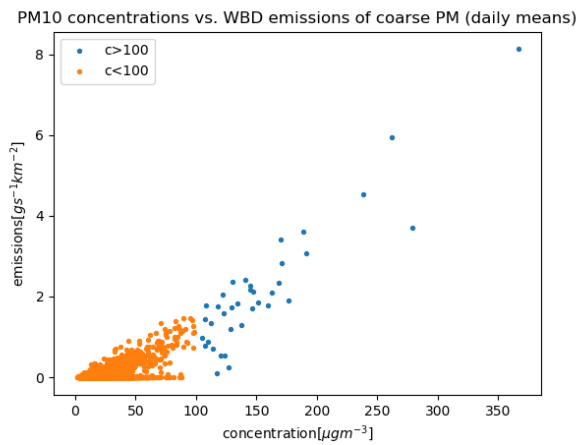


Figure 20. Scatter plot of the daily mean CAMx concentrations of PM10 corresponding to Prague center vs. WBD emissions of coarse PM (CCRS) from 90 km x 90 km area around Prague for the 2007-2016 period. Orange/blue circles stand for concentrations below/above $100 \mu\text{gm}^{-3}$

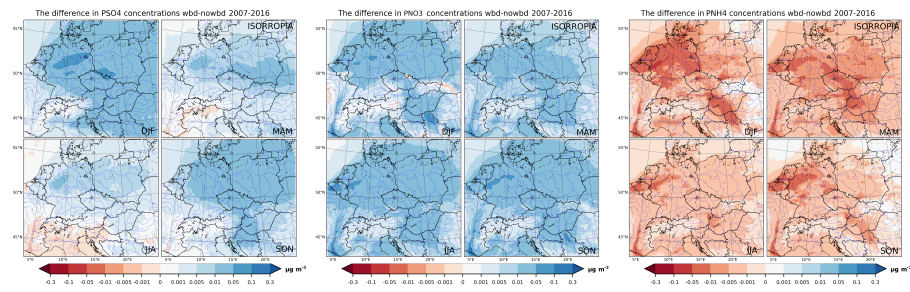


Figure 21. The WBD emission impact on secondary inorganic aerosol concentrations (PSO4, PNO3 and PNH4) with ISORROPIA, seasonally averaged, in μgm^{-3} for 2007-2016.

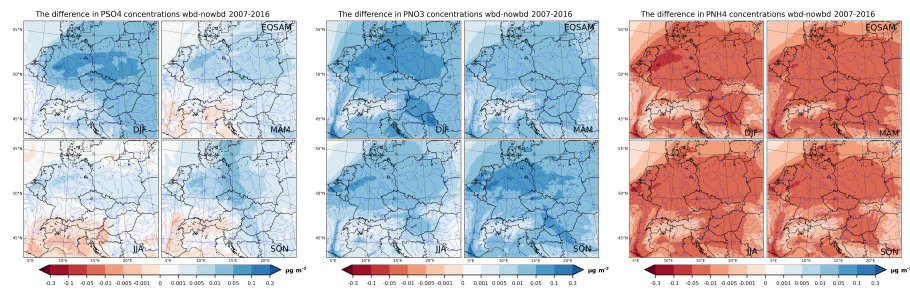


Figure 22. The WBD emission impact on secondary inorganic aerosol concentrations (PSO4, PNO3 and PNH4) with EQSAM, seasonally averaged, in μgm^{-3} for 2007-2016.

Impact of WBD emissions on urban PSO4 concentrations

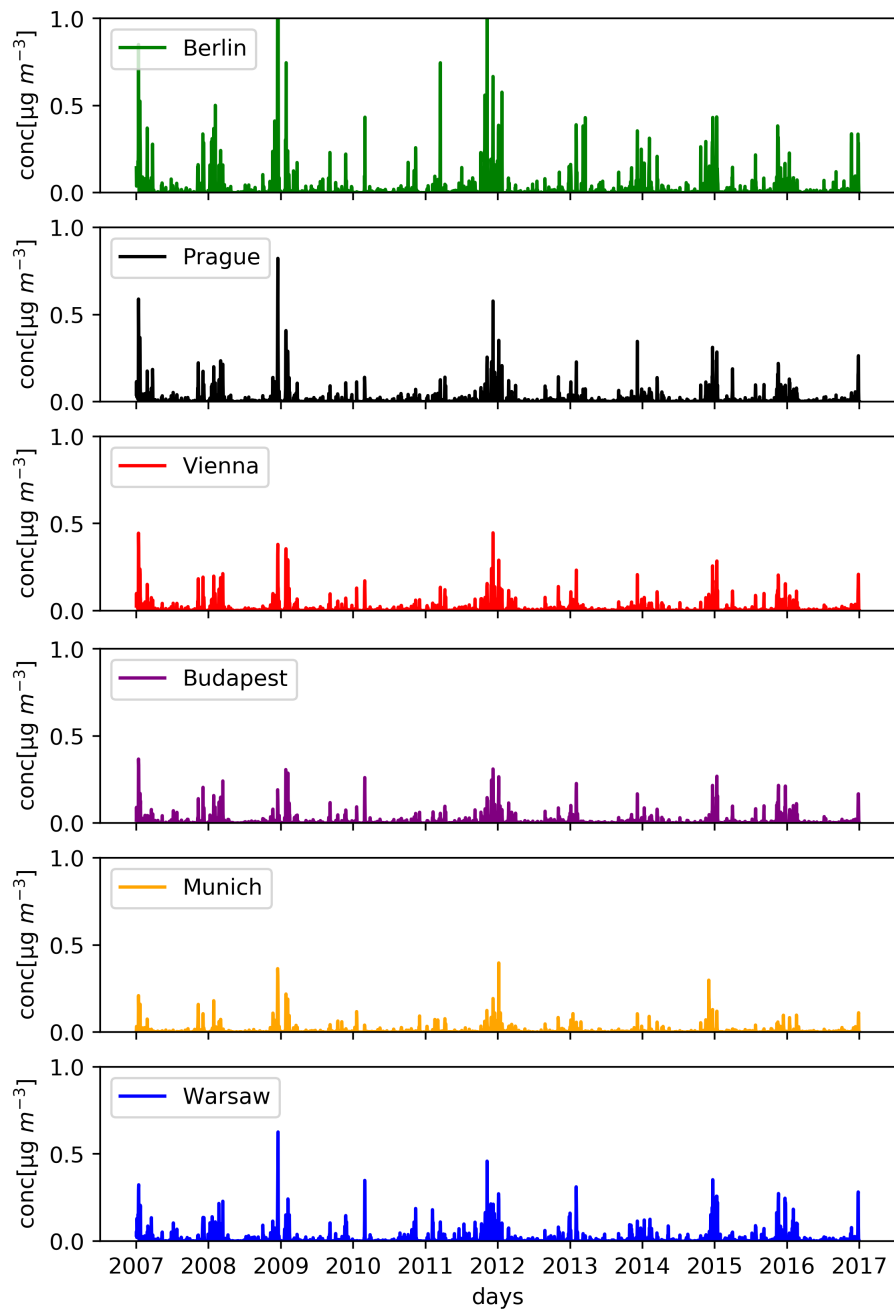


Figure 23. The long-term WBD impact on PSO4 concentrations in ISORROPIA, daily averaged for 2007-2016. Units in $\mu\text{g m}^{-3}$.

Impact of WBD emissions on urban PNO₃ concentrations

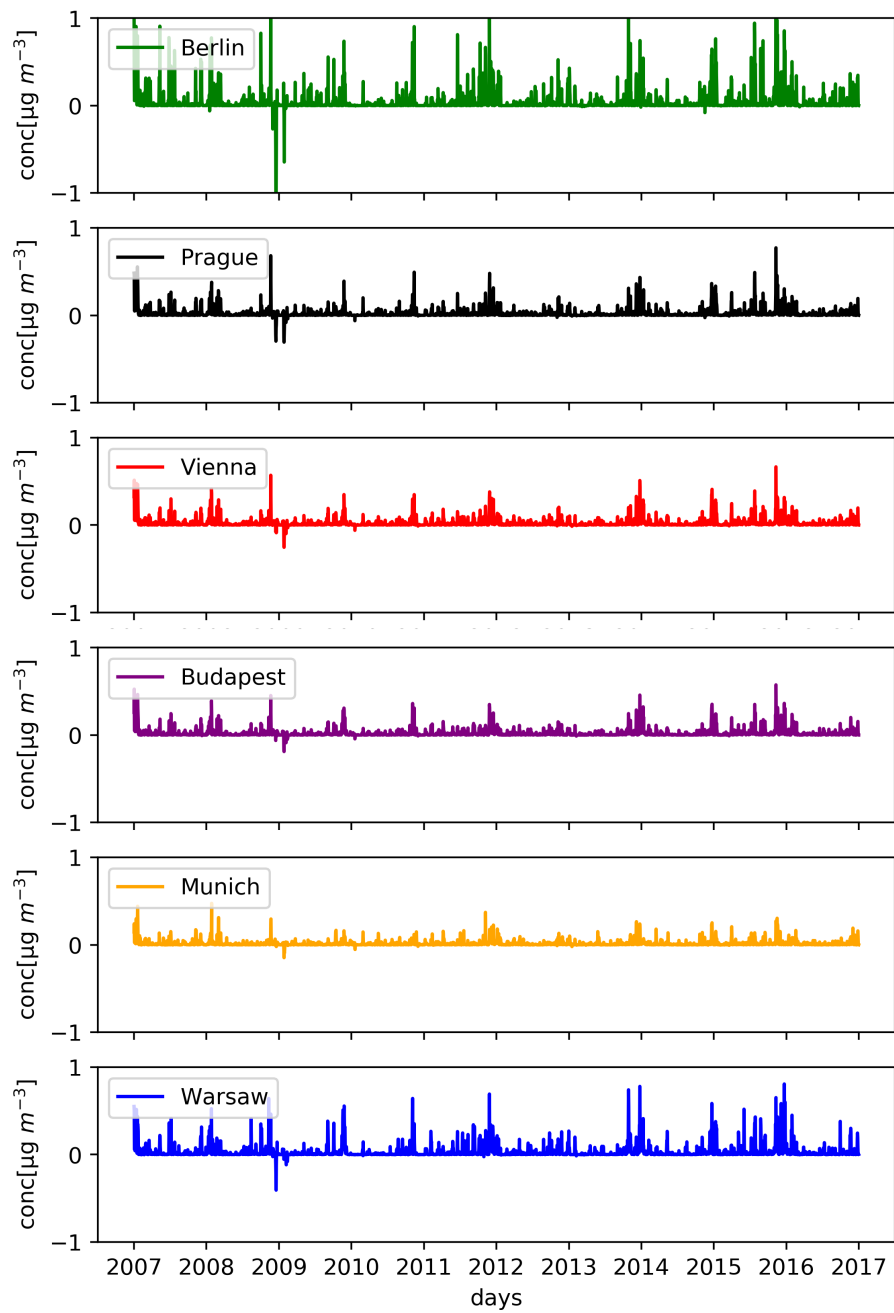


Figure 24. The long-term WBD impact on PNO₃ concentrations in ISORROPIA, daily averaged for 2007-2016. Units in $\mu\text{g m}^{-3}$.

Impact of WBD emissions on urban PNH4 concentrations

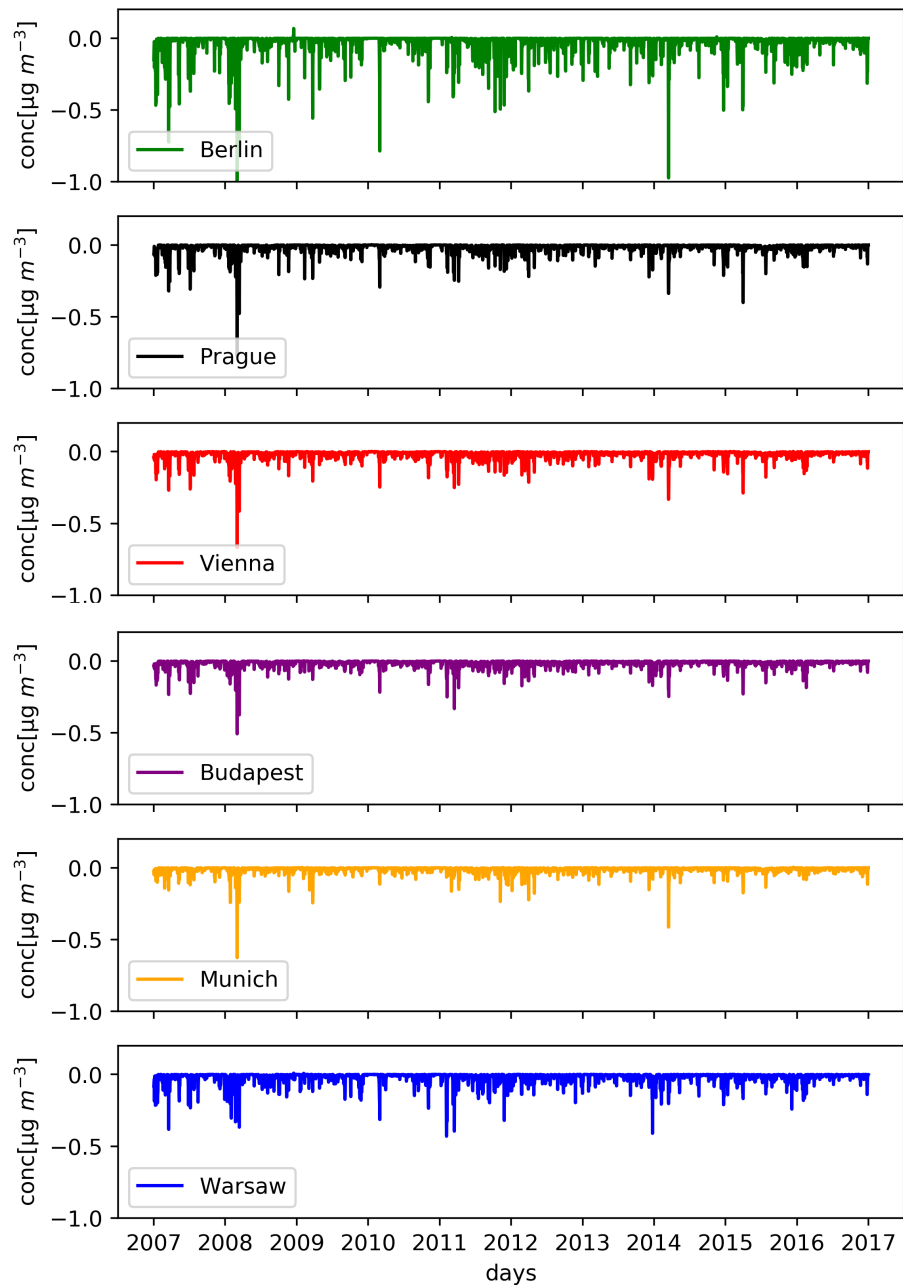


Figure 25. The long-term WBD impact on PNH4 concentrations in ISORROPIA, daily averaged for 2007-2016. Units in $\mu\text{g m}^{-3}$.

Table 1. Annual and seasonal statistical measures (Pearson correlation, RMSE, NMB) for PM2.5 for both WBD and noWBD ISORROPIA simulations calculated from the daily averages.

Cities	PM2.5	Pearson correlation		RMSE [μgm^{-3}]		NMB	
		WBD	noWBD	WBD	noWBD	WBD	noWBD
Vienna	Annual	0.6901	0.7146	9.6728	9.2239	0.0590	-0.0168
	DJF	0.6123	0.6628	12.7105	12.0459	0.0338	-0.0374
	MAM	0.6448	0.6852	9.5338	8.7539	0.1260	0.0539
	JJA	0.2534	0.3279	5.3553	5.1018	-0.1008	-0.1861
	SON	-0.1031	-0.1056	9.3356	9.3380	0.1069	0.0261
Prague	Annual	0.4778	0.6897	12.8227	9.4919	0.1088	-0.0748
	DJF	0.3349	0.6860	17.9578	12.5324	0.1639	-0.0674
	MAM	0.6195	0.7670	11.403	7.9885	0.1977	0.0405
	JJA	-0.0557	0.3106	6.8719	6.1530	-0.1450	-0.3323
	SON	0.4001	0.6020	12.8983	10.2484	0.1168	-0.0370
Berlin	Annual	0.6291	0.5342	10.7016	9.3405	-0.0340	-0.1321
	DJF	0.4985	0.6772	16.1053	13.5632	0.0242	-0.1036
	MAM	0.7176	0.7615	8.0587	7.4442	-0.0127	-0.0694
	JJA	0.1372	0.3264	5.9892	6.0888	-0.2928	-0.3792
	SON	0.6232	0.7338	10.0036	8.5933	0.0402	-0.0676
Munich	Annual	0.4612	0.6236	12.9249	9.6508	0.2983	0.1740
	DJF	0.4322	0.5893	17.1053	13.9096	0.3125	0.1935
	MAM	0.4533	0.7364	14.3441	7.8727	0.4240	0.2427
	JJA	0.1882	0.2981	5.6866	5.4625	-0.1405	-0.2118
	SON	0.4907	0.6378	11.6281	9.3698	0.4971	0.3857
Budapest	Annual	0.6893	0.7269	10.7620	10.5346	-0.1001	-0.1690
	DJF	0.6386	0.7330	15.6802	15.3078	-0.1673	-0.2432
	MAM	0.6209	0.6372	9.6156	9.4123	0.1270	0.0683
	JJA	0.2858	0.4302	7.3253	7.4711	-0.2976	-0.3852
	SON	0.6965	0.7488	10.0019	9.6213	-0.0883	-0.1473
Warsaw	Annual	0.5697	0.6999	14.4706	12.9026	-0.0922	-0.2027
	DJF	0.3858	0.5844	20.6196	18.0144	-0.0556	-0.1545
	MAM	0.5601	0.6769	12.5453	11.0780	-0.0504	-0.1512
	JJA	0.1074	0.2841	7.4900	7.7487	-0.2877	-0.3993
	SON	0.5116	0.6932	14.1531	12.6325	-0.0691	-0.2021

Table 2. Annual and seasonal statistical measures (Pearson correlation, RMSE, NMB) for PM10 for both the WBD and noWBD ISORROPIA simulations calculated from the daily averages.

Cities	PM10	Pearson correlation		RMSE [μgm^{-3}]		NMB	
		WBD	noWBD	WBD	noWBD	WBD	noWBD
Vienna	Annual	0.3836	0.6766	18.7462	13.1320	-0.0368	-0.2334
	DJF	0.2464	0.6456	23.9934	17.2384	0.0002	-0.1995
	MAM	0.3113	0.6709	20.0530	10.8410	0.0542	-0.1494
	JJA	0.1730	0.4334	11.8061	10.9038	-0.2901	-0.4682
	SON	0.4095	0.6471	16.9706	12.7993	-0.0028	-0.2011
Prague	Annual	-0.0221	0.6734	38.0248	13.1536	0.2422	-0.2729
	DJF	-0.1746	0.6618	51.8210	16.4792	0.3954	-0.2156
	MAM	0.1036	0.7397	36.9492	9.7224	0.3559	-0.1433
	JJA	-0.2398	0.3799	19.5380	12.1537	-0.0769	-0.5414
	SON	-0.0871	0.6478	35.9450	13.2200	0.1848	-0.2749
Berlin	Annual	0.1914	0.6675	23.2173	12.4793	0.0210	-0.2660
	DJF	0.0116	0.6662	35.7968	15.2236	0.2917	-0.1479
	MAM	0.4385	0.6820	14.6269	10.8560	-0.0592	-0.2295
	JJA	-0.0617	0.3630	13.7706	12.6158	-0.3419	-0.5571
	SON	0.1872	0.7033	22.0400	10.7076	0.0923	-0.1999
Munich	Annual	0.0310	0.5964	43.9461	11.2703	0.3812	-0.0682
	DJF	-0.0408	0.5701	60.0883	15.9116	0.5412	-0.0147
	MAM	0.0338	0.6998	53.9103	9.0543	0.5845	-0.0188
	JJA	-0.0714	0.3725	14.4982	9.0200	-0.1439	-0.3852
	SON	0.0447	0.5966	31.3270	9.7045	0.4013	-0.0724
Budapest	Annual	0.2518	0.5404	22.9692	19.7840	-0.2067	-0.3728
	DJF	0.0837	0.5737	28.0308	22.3826	-0.1267	-0.3159
	MAM	0.1778	0.4994	21.4223	14.2831	0.0082	-0.1924
	JJA	0.0900	0.2540	19.8013	20.5941	-0.4760	-0.6156
	SON	0.3210	0.6106	22.0720	20.9144	-0.2610	-0.3965
Warsaw	Annual	0.0882	0.6701	36.7845	16.7746	0.0725	-0.2971
	DJF	-0.0847	0.6332	53.4165	19.8648	0.2436	-0.1765
	MAM	0.1073	0.6210	33.1155	15.3840	0.0906	-0.2523
	JJA	-0.0759	0.4087	19.8315	15.5113	-0.2709	-0.5781
	SON	0.0182	0.6840	32.6067	15.8365	0.1072	-0.2739